RASSF8-mediated transport of Echinoid via the exocyst promotes *Drosophila* wing elongation and epithelial ordering

Eunice HY Chan[1*], Yanxiang Zhou[1], Birgit L Aerne[1], Maxine V Holder[1], Anne Weston[2], David J Barry[3], Lucy Collinson[2], Nicolas Tapon[1]

[1] Apoptosis and Proliferation Control Laboratory, The Francis Crick Institute, 1 Midland Road, London, UK

[2] Electron Microscopy Science Technology Platform, The Francis Crick Institute, 1 Midland Road, London, UK

[3] Advanced Light Microscopy Science Technology Platform, The Francis Crick Institute, 1 Midland Road, London, UK

Correspondence: nic.tapon@crick.ac.uk

* Present address: Aix Marseille University, CNRS, IBDM, Turing Center for Living Systems, Marseille, France

Keywords: Development, *Drosophila*, wing, cell junctions, epithelium, exocyst

Summary statement

Cell junction remodelling is essential for tissues to acquire their shape during development. RASSF8 is required for exocyst-mediated transport of the adherens junction component Echinoid to promote *Drosophila* wing elongation.

ABSTRACT

Cell-cell junctions are dynamic structures that maintain cell cohesion and shape in epithelial tissues. During development, junctions undergo extensive rearrangements to drive the epithelial remodelling required for morphogenesis. This is particularly evident during axis elongation, where neighbour exchanges, cell-cell rearrangements and oriented cell divisions lead to large-scale alterations in tissue shape. Polarised vesicle trafficking of junctional components by the exocyst complex has been

proposed to promote junctional rearrangements during epithelial remodelling, but the receptors that allow exocyst docking to the target membranes remain poorly understood. Here, we show that the adherens junction component Ras Association domain family 8 (RASSF8) is required for the epithelial re-ordering that occurs during *Drosophila* pupal wing proximo-distal elongation. We identify the exocyst component Sec15 as a RASSF8 interactor. *RASSF8* loss elicits cytoplasmic accumulation of Sec15 and Rab11-containing vesicles. These vesicles also contain the nectin-like homophilic adhesion molecule Echinoid, whose depletion phenocopies the wing elongation and epithelial packing defects observed in *RASSF8* mutants. Thus, our results suggest that RASSF8 promotes exocyst-dependent docking of Echinoid-containing vesicles during morphogenesis.

Introduction

The control of tissue shape during morphogenesis is one of the most complex questions in developmental biology. In epithelial tissues, cells adhere to each other through dynamic apical E-cadherin (Ecad)-containing adherens junctions (AJs) anchored to the underlying actin cytoskeleton (Charras and Yap, 2018; Rusu and Georgiou, 2020). Overall tissue shape is determined by polarised and coordinated cell behaviours such as oriented cell divisions and cell-cell rearrangements (Pare and Zallen, 2020; Perez-Vale and Peifer, 2020; van Leen et al., 2020). These planar polarised behaviours are driven by differential modulation of local actomyosin and adhesion dynamics, as well as large-scale tissue rearrangements. In *Drosophila* epithelia, the importance of polarised cell behaviours in tissue axis elongation has been demonstrated in several tissues, including the embryonic epidermis, notum and wing (Diaz de la Loza and Thompson, 2017; Mao and Lecuit, 2016; Pare and Zallen, 2020).

The proximo-distal (PD) extension of the *Drosophila* pupal wing has emerged as a powerful system in which to study epithelial remodelling (Diaz de la Loza and Thompson, 2017; Eaton and Julicher, 2011). The adult wing blade develops from a structure called the pouch in the wing imaginal disc. The wing disc is an epithelial sac in the larva that will give rise to the wing blade, the wing hinge (the connection

between the blade and thorax) and part of the thorax (Fig. 1A, upper panel) (Held, 2002). During the pupal stages of development, the wing blade acquires its final elongated shape through the contraction of the hinge (Fig. 1A) (Aigouy et al., 2010). Hinge contraction results in pulling of the wing blade against the resistance of the distal wing tip, which is tethered to the chitinous pupal cuticle via the apical extracellular matrix component Dumpy (Diaz-de-la-Loza et al., 2018; Etournay et al., 2015; Ray et al., 2015). This elongation causes both oriented cell divisions along the PD axis and widespread cell-cell rearrangements throughout the wing, ultimately reordering the wing cells from a relatively disorganised array of polygons to a highly regular hexagonal lattice (Fig. 1A, lower panel) (Aigouy et al., 2010; Classen et al., 2005; Diaz-de-la-Loza et al., 2018; Etournay et al., 2016; Etournay et al., 2015; Guirao et al., 2015; Ray et al., 2015).

Epithelial reordering during pupal wing elongation requires polarised actomyosin contractility and recycling of AJ components (Aigouy et al., 2010; Bardet et al., 2013; Classen et al., 2005; Ma et al., 2008; Warrington et al., 2013). The lipid phosphatase PTEN clears Rho-kinase and Myosin II from elongating junctions following neighbour exchanges (T1 transitions) and its depletion causes a failure of epithelial reordering (Bardet et al., 2013). Recycling of AJ components is thought to depend on the Frizzled (Fz) ”core” and Fat/Dachsous (Ds) planar cell polarity (PCP) signalling pathways (Aigouy et al., 2010; Classen et al., 2005; Gault et al., 2012; Ma et al., 2008; Warrington et al., 2013). The planar polarised seven-pass transmembrane protein Fz recruits Rho guanine nucleotide exchange factor 2 (RhoGEF2) via the scaffold protein Dishevelled (Dsh), which in turn promotes actomyosin-dependent Ecad endocytosis (Warrington et al., 2013). Flamingo (Fmi, also known as Starry night), another core PCP transmembrane protein, has been suggested to promote Ecad exocytosis in the pupal wing by recruiting the exocyst component Sec5 (Classen et al., 2005).

Polarised exocytosis is key to apico-basal polarity establishment and maintenance, as well as tissue remodelling (Polgar and Fogelgren, 2018; Roman-Fernandez and Bryant, 2016). The exocyst is an octameric protein complex first identified in yeast genetic screens for secretory mutants (TerBush et al., 1996; TerBush and Novick, 1995). The exocyst mediates docking of post-Golgi vesicles and Rab11-positive

recycling endosomes to the plasma membrane and promotes SNARE (Soluble NSF Attachment Protein Receptor) fusion complex activation (Heider and Munson, 2012; Zeng et al., 2017). Rab11 and the exocyst have been implicated in targeting vesicles and their cargoes to a variety of subcellular locations in higher eukaryotes, including the basolateral (Grindstaff et al., 1998; Lipschutz et al., 2000) and junctional/apical domains (Ahmed and Macara, 2017; Blankenship et al., 2007; Bryant et al., 2010; Campbell et al., 2009; Classen et al., 2005; Langevin et al., 2005; Mateus et al., 2011; Oztan et al., 2007; Xiong et al., 2012; Yeaman et al., 2004) in epithelial cells, the base of cilia (Lipschutz, 2019), the leading edge of migrating fibroblasts (Zago et al., 2019), nascent axonal tips (Lalli, 2009; Mehta et al., 2005; Murthy et al., 2003; Murthy et al., 2005) and photoreceptor rhabdomeres (Beronja et al., 2005; Satoh et al., 2005; Wu et al., 2005). Correctly delivering exocyst cargoes to these different locations is therefore crucial to maintain polarity and orderly developmental tissue remodelling.

Recognition of the correct target membranes is based both on interaction of the exocyst subunits Exo70 and Sec3 with phosphatidylinositol(4,5)-bisphosphate (He et al., 2007; Liu et al., 2007; Pleskot et al., 2015; Zhang et al., 2008), as well as binding of exocyst components to proteins localised at the target site. These proteins include small GTPases such as Cdc42 in yeast and higher eukaryotes (Zeng et al., 2017) or polarity determinants such as Par3 (Ahmed and Macara, 2017; Polgar and Fogelgren, 2018). However, for numerous exocyst target sites and cargoes, the nature of the docking cues is unknown.

We have previously identified the N-terminal RA (Ras Association) domain-containing protein RASSF8 as an AJ component required for morphogenesis during *Drosophila* retinal development (Langton et al., 2009). *RASSF8* mutants display cell adhesion defects as indicated by broken AJs during retinal remodelling (Langton et al., 2009). RASSF8 physically interacts with two other AJ-localised scaffold proteins, ASPP and Magi (Langton et al., 2007; Zaessinger et al., 2015). This complex promotes Ecad stability at AJs by recruiting the Par3 ortholog Bazooka (Baz) (Zaessinger et al., 2015) and antagonising Src activity via C-terminal Src kinase (Csk) (Langton et al., 2007; Langton et al., 2009). Intriguingly, RASSF8 also has ASPP-independent functions, since *RASSF8* mutant flies, unlike *ASPP* mutants, have a broad wing

phenotype, indicative of abnormal PD axis extension ((Langton et al., 2009) and this study). Here, we explore the functions of RASSF8 in wing development. We find that RASSF8 physically interacts with the exocyst component Sec15 and is required for trafficking of junctional components through Rab11 vesicles. Loss of *RASSF8* results in cytoplasmic accumulation of the adhesion molecule Echinoid (Ed) in enlarged Rab11-positive compartments. Furthermore, *ed* depletion in the wing blade leads to similar hexagonal packing and PD axis extension defects to those observed in *RASSF8* mutants. Thus, RASSF8 and Sec15 function together in promoting the Rab11-mediated trafficking of Ed during wing morphogenesis, suggesting that RASSF8, like its binding partner Baz/Par3, can act as an AJ receptor for exocyst-dependent membrane trafficking.

RESULTS

RASSF8 mutant wings have an abnormal aspect ratio and hexagonal packing defects

We previously reported that *RASSF8* mutant adult wings have both overgrowth and broad wing phenotypes (Langton et al., 2009). We quantified the shape defect by calculating the ratio between the antero-posterior (AP) and PD axes and observed a 20% increase in AP to PD ratio in *RASSF8* mutants (Fig. 1B-B'''). PD axis elongation during pupal wing development involves epithelial reordering induced by hinge contraction to yield a highly organised hexagonal lattice (Aigouy et al., 2010; Classen et al., 2005). To test whether *RASSF8* mutants present defects in this process, we imaged the AJs of wild type and *RASSF8* mutant pupal wings using an endogenously tagged *Ecad::GFP* knock-in line (Huang et al., 2009) and quantified the polygon distributions of the cell population between veins L4 and L5, distal to the posterior crossvein (Fig. 1A, purple rectangle) at 22, 26 and 30 hours after puparium formation (APF) (Fig. 1C-H). The polygon distribution indicates the number of neighbours of each individual cell, from tetragons (four neighbours) to octagons (eight neighbours). As previously reported (Aigouy et al., 2010; Classen et al., 2005), the proportion of hexagonal cells increases with time in wild type wings (Fig. 1C-D). At 30 hours APF, about 80% of cells achieved hexagonal packing (Fig. 1E). In contrast, the polygon distribution in *RASSF8* mutants remains relatively stagnant, with around 50% of cells

attaining a hexagonal shape at 30 hours APF (Fig. 1F-H). We observed a similar defect in cell packing across the L3 vein of the wing (Fig. 1A, green rectangle, Fig. S1A-E'). Analysis of *RASSF8* mutant clones suggests that this hexagonal patterning defect is cell-autonomous, since the surrounding wild type tissue is not affected (Fig. S1F-F''). Junctional Ecad intensity was not changed in *RASSF8* mutant pupal wing clones compared to control (Fig. S1F'''). Thus, RASSF8 is required for the maturation of the hexagonal lattice in the pupal wing.

The best characterised binding partner for RASSF8 is the scaffold protein ASPP, and both proteins function together during retinal morphogenesis (Langton et al., 2009). However, loss of *ASPP* results in a very mild hexagonal packing defect (~70% hexagons at 30 hours APF, Fig. S1G-K'), which may be due to the fact that junctional RASSF8 levels are reduced in ASPP mutant tissue (Langton et al., 2009). This suggests that RASSF8 acts independently of ASPP during wing morphogenesis.

RASSF8 interacts with Sec15 independently of Rab11

To explore the molecular mechanism by which RASSF8 controls hexagonal cell packing, we carried out a yeast-two hybrid screen using full-length *Drosophila* RASSF8 as a bait. In addition to ASPP, an established RASSF8 binding partner (Langton et al., 2009), we identified the exocyst subunit Sec15 (amino acids 59-234) as a RASSF8 interactor (Fig. 2A). To confirm this interaction, we co-expressed HA-tagged RASSF8 together with either Myc-tagged Sec15 or Sec5 in *Drosophila* S2 cells and performed co-immunoprecipitation (co-IP) experiments. We detected Sec15 but not Sec5 in the RASSF8 immunoprecipitates, confirming the RASSF8/Sec15 association (Fig. 2B). Sec15 binds the small GTPase Rab11 via its C-terminus, and this interaction is essential for polarised trafficking during sensory organ precursor (SOP) asymmetric division (Jafar-Nejad et al., 2005), in neurons (Mehta et al., 2005) and for AJ recycling of Ecad in the notum (Langevin et al., 2005). Since Rab11 inactivation prevents junctional remodelling and hexagonal packing in the pupal wing (Classen et al., 2005), we decided to further characterise the RASSF8/Sec15 interaction.

To map the domains required for the interaction between Sec15 and RASSF8, we carried out co-IP experiments using fragments of either protein. These experiments show that RASSF8 amino acids 350-490 are required for binding to Sec15, while the RA domain is dispensable (Fig. 2C, D). Sec15 amino acids 58-225 mediate binding to RASSF8 (Figures 2E, F), which is distinct from the Rab11 binding domain of Sec15 (amino acids 565-764) (Wu et al., 2005). Since previous studies had shown that Sec15 binds specifically to the GTP-bound form of Rab11 (Langevin et al., 2005; Wu et al., 2005; Zhang et al., 2004) and RASSF8 contains a RA domain, which could potentially bind to Ras family GTPases (Ponting and Benjamin, 1996), we tested whether RASSF8 and Rab11 can directly associate. While we detected a preferential binding of Sec15 to GTP-bound Rab11 (Fig. S2A), as previously described, no obvious interaction was detected between RASSF8 and Rab11 (GTP- or GDP-bound; Fig. S2B). Thus, our data suggest that RASSF8 interacts with the exocyst component Sec15, independently of Rab11.

Rab11 and Sec15 accumulate in *RASSF8* clones

As RASSF8 binds to Sec15, we tested whether the localisation of Rab11 or Sec15 is affected in *RASSF8* mutant clones. We observed cytoplasmic accumulation of Sec15::GFP (expressed under the *ubiquitin-63E* promoter – see materials and methods) and Rab11 in *RASSF8* clones at various time points (Fig. 3A-F”). In the case of Sec15, the heterozygous tissue already displayed a marked cytoplasmic accumulation, showing that Sec15 is extremely sensitive to RASSF8 dosage and supporting the idea that these proteins physically interact. In agreement with what has been described in the pupal notum (Langevin et al., 2005), we observed an accumulation of intracellular Rab11 within Sec15 mutant clones in the pupal wing (Fig. 4A-A’’). Together with the fact that dominant negative Rab11 also prevents hexagonal packing (Classen et al., 2005), this suggests that RASSF8 is required for exocyst-dependent trafficking of Rab11 vesicles.

In budding yeast, some exocyst subunits (Sec3p and Exo70p) are at the exocytosis target site, while others are associated with the cargo vesicle, suggesting that full exocyst assembly occurs at the membrane upon vesicle docking (Boyd et al., 2004;

Liu et al., 2018). Indeed, in *Drosophila*, Sec15 is primarily vesicular (Jafar-Nejad et al., 2005; Langevin et al., 2005), while several other subunits (Sec5, Sec6, Sec8) are at least partly membrane-associated (Beronja et al., 2005; Langevin et al., 2005; Murthy et al., 2005). Interestingly, the localisation of Sec5, which is primarily cortical in the pupal wing, is not altered in *RASSF8* mutant clones, suggesting that RASSF8 is required for the localisation of a subset of exocyst components (Fig. 4B-B').

We have previously shown that *RASSF8* mutant clones have patterning defects in retinal development at the pupal stage (26-27 hours APF) (Langton et al., 2009). In this system, we also observed Sec15 and Rab11 accumulation in *RASSF8* mutant clones, suggesting that the RASSF8 requirement for exocyst function is not confined to the wing (Fig. 4C-D''). In contrast, the markers of early endosomes (Rab5) and mature endosomes (Rab7, Hrs) are not altered in *RASSF8* retinal clones, showing that the Sec15/Rab11 defect is not indicative of a general disruption in vesicle trafficking (Fig. S3A-C''). Consistent with a defect in cell-cell contacts, transmission electron microscopy (TEM) of pupal retinas revealed gaps between *RASSF8* mutant cells (Fig. S4A-E).

RASSF8 is implicated in exocyst function independently of Bazooka/Par3

Together, our findings are consistent with a subset of Rab11 vesicles failing to be correctly targeted to the plasma membrane in *RASSF8* mutants. Since RASSF8 is localised at the cell cortex (AJs) in the wing and eye (Langton et al., 2009), this suggests that RASSF8 may act as a cortical receptor for exocyst docking. Interestingly, the polarity protein Par3 has recently been shown to act as an exocyst receptor in mouse mammary epithelial cells by interacting directly with Exo70 (Ahmed and Macara, 2017). This warranted further investigation since ASPP2, the mammalian homolog of the RASSF8 partner ASPP, has been reported to associate with Par3 (Cong et al., 2010; Sottocornola et al., 2010). In addition, we had reported that a complex comprising the scaffold protein Magi, ASPP and RASSF8 is required for the correct recruitment of the Par3 ortholog Baz to the AJs during retinal morphogenesis (Zaessinger et al., 2015). Finally, we showed that the RASSF8 paralog Meru directly binds to Baz to induce its planar polarisation in *Drosophila* Sensory

Organ Precursor cells (Banerjee et al., 2017). This suggests that N-terminal RASSF proteins have a general function in Par3/Baz recruitment.

Indeed, our RASSF8 two-hybrid screen identified the Baz N-terminus (a.a. 132-263) as a RASSF8 interaction partner. In S2 cell co-IP experiments, RASSF8 could associate with Baz (Fig. 4E), while ASPP could only co-precipitate Baz only in the presence of RASSF8 (Fig. 4F). This indicates that the Magi/ASPP/RASSF8 complex can associate with Baz via a direct interaction between RASSF8 and Baz. Given the implication of Par3 as an exocyst receptor in mammalian cells (Ahmed and Macara, 2017), we tested if loss of Baz leads to a mislocalisation of Rab11 vesicles in fly tissues. However, we observed only modest (1.1-fold) cytoplasmic Rab11 accumulation in the pupal wing (Fig. S4F-G) in *baz* mutant clones compared to 1.62-fold for *RASSF8* mutants (Fig. 3E-E'' and 5A-C). This indicates that RASSF8 is required for trafficking of Rab11 vesicles independently of Baz in the pupal wing.

Echinoid is a cargo of RASSF8/Sec15/Rab11 mediated transport

Since our result suggested that RASSF8 is required for docking of Rab11 vesicles to the plasma membrane, we wished to identify the cargo(es) present in the stranded vesicles that accumulate in *RASSF8* mutant tissue. The exocyst has been implicated in Ecad trafficking in the fly notum (Langevin et al., 2005) and pupal wing (Classen et al., 2005), as well as in mammalian epithelial cells (Ahmed and Macara, 2017; Xiong et al., 2012; Yeaman et al., 2004). However, Ecad did not accumulate in intracellular vesicles in *RASSF8* mutant clones (Fig. S1F-F''). We examined the localisation of several transmembrane proteins involved in AJ maintenance and signalling (see Materials and Methods for details). The majority of these, such as the core PCP component Fmi (Fig. S4H-H'') were not affected. Using this candidate approach, we found that Echinoid (Ed) is accumulated in a punctate pattern in *RASSF8* clones at the AJs and in the cytoplasm (Fig. 5A-B'').

Ed is a large immunoglobulin (Ig) repeat trans-membrane homophilic adhesion molecule that cooperates with Ecad to mediate cell adhesion and sorting via the actomyosin network (Ho et al., 2010; Islam et al., 2003; Laplante and Nilson, 2006; Wei et al., 2005). Ed presents functional similarities to mammalian nectins: both are junctional components that belong to the Ig superfamily and recruit the F-actin binding protein Canoe (afadin in mammals), but as their domain structure differs, Ed is considered nectin-like rather than being a nectin ortholog (Mandai et al., 2013; Wei et al., 2005). Ed has previously been observed to colocalise with early Rab5, late Rab7 and recycling Rab11 endosomal vesicles (Fetting et al., 2009; Li et al., 2015; Rawlins et al., 2003a). Since Rab11 but not Rab5-/7-positive vesicles accumulate in *RASSF8* mutant clones (Fig. 3, 4), we performed colocalisation analysis of Rab11 and Ed (Fig. 5B-D and Materials and Methods). Confirming our previous results, we observed that Rab11 compartments accumulate in *RASSF8* mutant clones (Fig. 5C; 1.62-fold increase in cytoplasmic Rab11 compared to control). Furthermore, there was a significant increase in Rab11/Ed colocalisation in *RASSF8* clones (Fig. 5D), suggesting that Ed trafficking by Rab11 is perturbed in *RASSF8* mutants. Ed was present in enlarged Rab11 compartments both in the cytoplasm and close to the apical plasma membrane, consistent with a failure to fuse with the junctions (Fig. 5B-B'').

We wished to test whether, like RASSF8, Ed is required for wing elongation and hexagonalisation. *ed* mutant clones trigger the formation of an acto-myosin cable in neighbouring wild type cells, which often leads to their exclusion from the wing disc epithelium (Wei et al., 2005), making recovery of clones at the pupal stage difficult. However, we can partially inhibit Ed function in the wing blade by driving an RNAi construct under the *nubbin-GAL4* (*nub-GAL4*) driver. Similar to *RASSF8* mutants, *ed* depletion in the wing blade leads to an increase in the AP/PD ratio (Fig. 5E-F). Furthermore, we observed a defect in hexagonal packing in *ed*-depleted wings compared with control (at 30 hours APF, control: 73%, *ed*-depleted: 60%) (Fig. 5G-L). Thus, loss of Ed elicits similar pupal wing phenotypes to RASSF8 loss, consistent with the model that RASSF8 is required for Ed AJ trafficking during wing morphogenesis.

DISCUSSION

The accurate and timely remodelling of epithelial tissues is a key feature of organogenesis (Harris and Tepass, 2010). Here, we explore the function of the RA domain-containing scaffold protein RASSF8 in epithelial morphogenesis using pupal wing development. We show that RASSF8 functions in this process independently of its partner ASPP, with which it regulates Src activity at the AJs (Langton et al., 2009) (Fig. S1). Our work reveals that RASSF8 is required for remodelling of the wing epithelium to a mature hexagonal lattice (Fig. 1, S1), a process dependent on planar polarised acto-myosin contractility and recycling of junctional components (Aigouy et al., 2010; Bardet et al., 2013; Classen et al., 2005; Gault et al., 2012; Ma et al., 2008; Warrington et al., 2013).

We identified the exocyst component Sec15 as a binding partner for RASSF8 (Fig. 2). As Sec15 is required for recycling of Ecad from the basal membrane back to the AJs in the pupal notum (Langevin et al., 2005) and inhibition of its binding partner Rab11 prevents pupal wing hexagonalisation (Classen et al., 2005), we investigated the consequences of RASSF8 loss on exocyst function. We found that Sec15 and Rab11, but not Sec5, accumulate in the cytoplasm of *RASSF8* mutant cells (Fig. 3), consistent with the idea that RASSF8 acts as an AJ receptor that allows exocyst-dependent docking of Rab11 vesicles prior to fusion with the target membrane.

RASSF8-mediated trafficking of Echinoid vesicles

Although Ecad-positive REs accumulate in *sec15* mutant tissue in the pupal notum (Langevin et al., 2005), we observed no such accumulation in *RASSF8* mutant cells (Fig. 1, S1). This suggests that RASSF8 is not involved in trafficking of Ecad endosomes. Instead, we identified the Ig superfamily adhesion molecule Ed as a cargo whose delivery is dependent on RASSF8 (Fig. 5). The exocyst and Rab11 are involved in both biosynthetic and recycling trafficking (Heider and Munson, 2012), therefore RASSF8 could promote the delivery of newly synthesised and/or recycled Ed to the junctions. Ed depletion in the wing results in similar, though less pronounced, hexagonalisation and wing elongation defects to *RASSF8* mutants, suggesting that the *RASSF8* phenotype is at least in part due to defective Ed

trafficking (Fig. 5). Interestingly, mammalian nectin-2α has been implicated in exocyst apical recruitment in MDCK cells (Yeaman et al., 2004), but ours is the first report of a nectin-like molecule as an exocyst cargo. With respect to the lack of Ecad cytoplasmic accumulation in *RASSF8* mutants, it is also worth noting that exocyst dependency of trans-membrane cargoes is tissue-specific. For instance, trafficking of the polarity protein Crumbs requires the exocyst in the embryonic epidermis (Blankenship et al., 2007; Roeth et al., 2009) and follicular epithelium (Aguilar-Aragon et al., 2020), but not in the pupal notum (Langevin et al., 2005), photoreceptors (Beronja et al., 2005) and renal tubules (Campbell et al., 2009).

How could disruptions in Ed trafficking lead to epithelial reordering defects? Like many Ig superfamily molecules, Ed can *trans*-dimerise (Islam et al., 2003; Rawlins et al., 2003a). Ed is also associated with the acto-myosin cytoskeleton via a direct interaction with the actin filament binding protein Canoe (Wei et al., 2005). So far, the majority of Ed functions have been related to cell sorting at Ed expression boundaries. Indeed, at the boundary of *ed* mutant clones, Ed is lost from the junctions of wild type cells that abut the mutant clones, inducing the assembly of a contractile acto-myosin cable that leads to apical constriction of the mutant cells (Wei et al., 2005). Acto-myosin contractility at the clone border, together with differential adhesion, leads to a cell sorting phenotype characterised by a smooth border between the mutant and wild type populations (Chang et al., 2011). Naturally occurring Ed expression boundaries can also trigger acto-myosin cable formation and drive cell sorting events in several morphogenetic processes, such as dorsal closure (Laplante and Nilson, 2006; Lin et al., 2007), ommatidial rotation (Fetting et al., 2009; Ho et al., 2010) and ovarian follicle cell segregation (Laplante and Nilson, 2006). However, as we did not observe any Ed expression boundaries in the pupal wing, and *RASSF8* mutant clones do not display the characteristic round smooth border of *ed* mutant clones, Ed's role in hexagonalisation is likely to be distinct. Whether this role involves cytoskeletal modulation or an Ed adhesive function through homophilic association or heterophilic interactions with other partners such as its paralog Friend of Echinoid (Ozkan et al., 2013) remains to be investigated. Alternatively, as Ed has been shown to modulate several signalling pathways, such as Notch (Chandra et al.,

2003; Escudero et al., 2003; Rawlins et al., 2003a), Hippo (Yue et al., 2012) and Epidermal growth factor receptor (Bai et al., 2001; Fetting et al., 2009; Islam et al., 2003; Rawlins et al., 2003b; Spencer and Cagan, 2003), it may be acting via cell-cell signalling.

Junctional targeting of the exocyst

Structural analyses of the yeast exocyst have shown that the full octameric complex can be subdivided into two distinct subcomplexes, with subcomplex I composed of Sec3/5/6/8, while complex II contains Sec 10/15 and exo70/84 (Ganesan et al., 2020; Heider et al., 2016; Mei et al., 2018). Macara and colleagues have recently shown that in mammalian cells, the two subcomplexes can arrive at the plasma membrane following different kinetics, suggesting that these can be recruited to the target membrane via independent mechanisms (Ahmed et al., 2018). Our data indicate that RASSF8 loss disrupts the localisation of Sec15 (subcomplex II), while Sec5 (subcomplex I) is not affected (Fig. 3, 4). Interestingly, numerous lines of evidence show that subcomplex II plays a key role in exocyst targeting to the adherens/tight junctions. Indeed, binary associations between Exo70 and Par3 (Ahmed and Macara, 2017), Sec10 and Par6 (Zuo et al., 2011) or Armadillo/β-catenin (Langevin et al., 2005), Exo84 and Par6 (Das et al., 2014), or Sec15 and RASSF8 (this study) have been reported. This diversity of exocyst recruitment mechanisms may reflect the diverse nature of cell-cell contacts across different tissues and developmental stages. In the pupal wing, RASSF8 appears to play a more essential role in Rab11 vesicle trafficking than its binding partner Baz/Par3 (Fig. 5, S4), but it would be interesting to know if the different exocyst subcomplex II/junctional component interactions are differentially required according to cell type, context and cargo. Understanding how specific interactions of the exocyst with target membranes ensures accurate sorting of adhesion molecules to the appropriate subcellular localisation in the correct spatial and temporal pattern is key to understanding how epithelial tissues are built, remodelled and maintained.

MATERIALS AND METHODS

Drosophila stocks

FRT82B Sec15^{1} was a gift from Hugo Bellen (Mehta et al., 2005), *DEcad::GFP* was a gift from Yang Hong (Huang et al., 2009), *baz*^{eh747} *FRT19A* was a gift from Andreas Wodarz (Eberl and Hilliker, 1988). *RASSF8*^{6} (Langton et al., 2009) and *ASPP*^{8} (Langton et al., 2007) were previously described. *ubi-Sec15::GFP* transgenic flies were generated by introducing the Sec15 gene into a modified pKC26 plasmid containing the *ubiquitin-63E* promoter and a C-terminal GFP tag (Zaessinger et al., 2015). This vector was injected by Bestgene Inc. (Chino Hills, USA) into flies bearing a 3L *attP* landing site (VIE-217). *ed-RNAi* (BL-38243) and *Df(3R)BSC321* (BL-24909) were obtained from the Bloomington *Drosophila* Stock Centre.

Genotypes

Fig. 1B, S4A-A'': *w*^{iso}

Fig. 1B': *w;; RASSF8*^{6}

Fig. 1B": *w;; RASSF8*^{6}*/Df (3R)BSC321*

Fig. 1C-D", Fig. S1A-B", G-H'': *w; Ecad::GFPki*

Fig. 1F-G", Fig. S1C-D'': *w; Ecad::GFP; RASSF8*^{6}*/RASSF8*^{6}

Fig. 3A-C''': *hsFlp;; FRT82B ubi nlsRFP/ ubi-Sec15::GFP, FRT82B RASSF8*^{6}

Fig. 3D-F'' *hsFlp;; FRT82B ubiGFP/FRT82B RASSF8*^{6}

Fig. 4A-A": *hsFlp;; FRT82B ubiRFP/FRT82B Sec15*^{1}

Fig. 4B-B'', 5A-B": *hsFlp;; FRT82B ubi nlsRFP/FRT82B RASSF8*^{6}

Fig. 4C-D';, Fig. S3A-C'': *eyFlp;; FRT82B ubiGFP/ FRT82B RASSF8*^{6}

Fig. 5E, Figure 5G-H": *w; nub-Gal4/UAS-RFP;*

Fig. 5E', Figure 5I-J": *w; nub-Gal4/UAS-ed RNAi (TRiP.HMS01687);*

Fig. S1I-J": w; *Ecad::GFP, ASPP*^{8}*;*

Fig. S1F-F", S4H-H'': *hsFlp; Ecad::GFPki/+; FRT82B ubi myr-RFP/FRT82B RASSF8*^{6}

Fig. S4F-F'': *baz*^{eh747} *FRT19A/ubi-RFP, hsFLP FRT19A*

Yeast two-hybrid

The yeast two-hybrid screen with full-length RASSF8 cloned as an N-terminal LexA fusion in pB29 as bait was performed by Hybrigenics SA (Paris, France) using a *Drosophila* whole embryo cDNA collection (RP2).

Plasmid construction

The *Sec15* gene was amplified from DGRC cDNA clone RE55430. Genes of interest were cloned into Gateway entry vector and subsequently expression vectors containing HA/Myc tags (*Drosophila* Gateway Vector Collection - http://emb.carnegiescience.edu/labs/murphy/Gateway%20vectors.html).

Small GTPases used for in vitro GST pulldown assay were reverse-transcribed from total mRNA isolated from wild type adult flies, cloned into the pGEX4T-1 vector and verified by sequencing.

GST fusion protein expression

Small GTPases were expressed in BL21(DE3)pLysS bacteria (Promega). Protein expression was induced with 0.5 mM Isopropyl β-D-1-thiogalactopyranoside (IPTG) and carried out at 18°C overnight. Bacteria were lysed by sonication in LyBTL (50 mM Tris HCl pH 7.5, 50 mM NaCl, 5 mM $MgCl_2$, 0.1% [v/v] Triton X-100) buffer containing 1mM DTT, 1mM PMSF, 0.5 g/L lysozyme and Protease Inhibitor Cocktail (Roche, Lewes, UK). The supernatant was incubated with glutathione Sepharose 4B beads (GE Healthcare) at 4 °C for 1 hour.

***In vitro* binding assay for small GTPases**

Glutathione Sepharose beads with 60 µg small GTPases were loaded with GTPγS or GDP in GTPase loading buffer (20 mM HEPES pH 7.5, 25 mM NaCl, 10 mM EDTA, 2 mM GTP/ GTPγS) for 20 minutes at 37 °C. NL100 buffer (20 mM HEPES pH 7.5, 100 mM NaCl, 5 mM MgCl2, 0.1% [v/v] Triton X-100) containing 0.1 mM GTPγS or GDP was added immediately afterwards to stop nucleotide exchange. S2 cell lysate was added to the beads in NL100 buffer. The binding was performed at 4 °C for one hour.

Western blotting and co-IP assays

S2-DGRC cells (Cellosaurus CVCL_TZ72) were obtained from the *Drosophila* Genomics Resource Center (NIH Grant 2P40OD010949) and transfected with Effectene (Qiagen). For co-IP assays, cells were lysed in HEPES lysis buffer (50 mM HEPES pH7.4, 150 mM NaCl, 0.5% [v/v] Triton X-100) supplemented with phosphatase inhibitor cocktails 1 and 2 (Sigma), and Protease Inhibitor Cocktail (Roche) on ice for 15 mins. Soluble cell lysates were obtained after centrifugation at 15,000 *x g* for 15 mins at 4 °C. Protein concentrations were determined using the Dc protein assay (Bio-Rad). Lysates were then incubated with Protein A/G sepharose beads and appropriate antibodies for 2 hours at 4 °C. Immunoprecipitates were then purified after washing 4 times with HEPES lysis buffer. Detection of purified proteins and associated complexes was performed by immunoblot analysis using chemiluminescence (GE Healthcare). Western blots were probed with anti-FLAG (mouse M2, Sigma), anti-Myc (mouse 9E10, Santa Cruz Biotechnology), anti-HA (rat 3F10, Roche), anti-RASSF8 (Langton et al., 2009).

Electron Microscopy and image analysis

Dissected pupal retinas were fixed in 4 % formaldehyde and 1.5 % glutaraldehyde in 0.1 M phosphate buffer for 1 hour at room temperature. Samples were further fixed with reduced osmium tetroxide for 1 hour followed by 1 % tannic acid in 0.05 M sodium cacodylate for 45 mins. Samples were then dehydrated through a graded series of ethanol, embedded in Epon resin and sectioned at 70 nm using an Ultracut UCT ultramicrotome (Leica Microsystems) and post-stained with lead citrate. Images were obtained with a Tecnai G^2 Spirit transmission electron microscope (FEI Company, Hillsboro, US) and an Orius CCD camera (Gatan). Images of ommatidia were taken from the apical plane. Non-overlapping images from a single plane were used to quantify gaps in the cell-cell junctions (n=17) using manual segmentation in Amira software (Visage Imaging). A projection of the segmented gaps from overlaid, but non-sequential, images illustrates the increase in gaps in the mutant over the wild type.

Quantification of the number of neighbours of each cell in pupal wing

Z projections of pupal wings labelled with Ecad::GFP or fluorescently labelled anti-Arm antibodies were created by ImageJ. The number of neighbours of each cell was quantified using the Packing Analyzer (v2.0) described in (Aigouy et al., 2010).

Quantification of Ed and Rab11 colocalisation

Quantification of Rab11 expression or colocalisation of Ed with Rab11 was achieved using a FIJI Plugin called Particle Mapper:
https://github.com/djpbarry/CALM/wiki/Particle-Mapper (See (Wanaguru et al., 2018) for details). However, because Particle Mapper requires a nuclear marker as one of its inputs, additional processing was required in order to generate a pseudo-nuclear channel for the purposes of this study.

Pseudo-nuclear markers were generated as follows. Multi-channel confocal image stacks were first analysed to identify and isolate the highest contrast z-position. Subsequently, the Echinoid channel at this z-location was isolated and noise and background were suppressed. Grey-level thresholding was then used to generate a binary image, which was subsequently skeletonised and pruned. The resultant inter-skeleton regions, following an erosion operation, were assumed to be reasonable approximations of the cell interiors. A FIJI script to automate all of these steps is available online:
https://github.com/djpbarry/wing-cell-quant/blob/main/Rab11_quant.cppipe
For the data presented in this paper, the script default options were used. At least 31 cells per genotype were analysed from three different retinas. The analysis was done in single confocal sections (0.5 µm in depth) at the level of the adherens junctions.

Quantification of Ecad at cell junctions

Quantification of Ecad intensity at cell-cell junctions was achieved using a combination of a FIJI script:
https://github.com/djpbarry/wing-cell-quant/blob/main/Blob_Detector.ijm
and a CellProfiler pipeline:
https://github.com/djpbarry/wing-cell-quant/blob/main/Ecad%20in%20F8%20clones.cppipe

Briefly, the locations of cell centres were estimated in FIJI using a blob detection approach based on calculation of Hessian eigenvalues: https://imagescience.org/meijering/software/featurej/hessian

These centre locations were then used to seed a full cell segmentation using MorphoLibJ's marker-controlled watershed (Legland et al., 2016).

The resultant cell segmentations were then analysed using the CellProfiler pipeline. Cells were first filtered based on size and Ecad intensity to remove those likely to be coincident with veins, which have elevated Ecad density and could have biased the results. The Ecad intensity at the cell periphery was then quantified per cell across wild type and *RASSF8* mutant populations.

Analysis of *Drosophila* wing roundness

For analysis of wing roundness, young adult wings were processed, mounted and imaged as described (Ribeiro et al., 2010). The roundness of the wing is defined by the length of AP axis along the L3 vein divided by the length of the PD axis crossing the posterior crossvein.

Genetics and immunochemistry

Mosaic tissues were obtained using the FLP/FRT system with *hsFlp*. Flies were heat-shocked for 60 mins at 48 hours and 72 hours after egg deposition. Pupae were staged by collecting white prepupae 3 days after the first heat-shock and incubating at 25 °C for the indicated times. Pupal wings and retinas were fixed in 8 % and 4 % paraformaldehyde in PBS respectively for 30 mins (larval wing discs in 4 % paraformaldehyde in PBS for 30 mins), washed 3 times with PBS, permeabilised with PBT (PBS + 0.3 % Triton x100), blocked with PBT + 1 % BSA, immunostained with the indicated primary antibodies in PBT + 1 % BSA at 4 °C overnight and secondary antibodies for 2 hours at room temperature.

Primary antibodies used were rabbit anti-Rab5, anti-Rab7, anti-Rab11 (1:2000, gifts from Akira Nakamura; (Tanaka and Nakamura, 2008)), guinea pig anti-Sec15 and anti-Hrs (1:1000, gift from Hugo Bellen; (Lloyd et al., 2002; Mehta et al., 2005)), rat anti-Ed (1:1000, gift from Jui-Chou Hsu (Wei et al., 2005)), mouse anti-Sec5 (22A2) antibody (1:200, gift from Thomas Schwartz; (Murthy et al., 2003)). The rat anti DE-cadherin (1:100, developed by T. Uemura), mouse anti-Arm (1:100, developed by E. Wiechaus) and anti-Fmi #74 (1:20, Developed by T. Uemura) were obtained from the Developmental Studies Hybridoma Bank, created by the NICHD of the NIH and maintained at The University of Iowa, Department of Biology, Iowa City, IA 52242. Secondary antibodies used were rhodamine red-X donkey anti-rabbit, anti-rat, and anti-mouse, fluorescein isothiocyanate (FITC) donkey anti-rabbit, anti-rat, and anti-mouse (Jackson ImmunoResearch, Newmarket, UK), goat anti-rat Alexa 647, and goat anti-rabbit Alexa 633, all at 1:500. Fluorescence images were acquired with a Zeiss LSM780 or a Zeiss LSM880 confocal.

Antibodies against transmembrane proteins tested for accumulation in *RASSF8* mutant clones: mouse anti-Fmi (1:20, DSHB Flamingo #74), rabbit anti-Ds (1:1000, from David Strutt (Strutt and Strutt, 2002)), mouse anti-Roughest/IrreC (1:10, from Karl-Friedrich Fischbach; (Schneider et al., 1995)), mouse anti-Notch-ICD (1:100, DSHB C17.9C6; deposited by S. Artavanis-Tsakonas), rat anti-Crb (1:1000, from Franck Pichaud; (Walther et al., 2016)), rat anti-Fat (1:1000, from Helen McNeill), rabbit anti-EGFR (1:1000, from Erika Bach), rat anti-SNS (1:1000, from Susan Abmayr; (Bour et al., 2000)), rat anti-Hibris (1:1000, from Tetsuya Tabata; (Sugie et al., 2010)), rat anti-Kirre (1:1000, from Susan Abmayr; (Galletta et al., 2004)).

Statistics

Statistical analysis was performed using Prism (GraphPad Software). All raw data and details of statistical tests are in Tables S1 and S2. All averages correspond to mean.

Acknowledgements

We are grateful to H. Bellen, S. Eaton, T. Schwartz, Y. Hong, A. Wodarz, D. Strutt, H. McNeill, S. Abmayr, KF. Fischbach, F. Pichaud, E. Bach, A. Nakamura, the Bloomington *Drosophila* Stock Center and the DSHB for antibodies and fly stocks. We thank B. Aigouy for Packing Analyzer (v2.0). We thank members of the Tapon lab, A. Chalmers and members of his lab for helpful discussions, P. Jordan from the Crick Advanced Light Microscopy science technology platform for microscopy advice, T. Gilbank, S. Maloney and F. Earl for fly stock maintenance. We are grateful to M. McLellan, I. Gailite and P. Ribeiro for critical reading of the manuscript. E.H.Y. Chan thanks P.F. Lenne and F. Schnorrer for their support.

Competing interests

The authors declare no competing interests.

Funding

E.H.Y. Chan was supported by Marie Curie long-term fellowship (IEF2008 no. 237404) and the Francis Crick Institute. Work in the Tapon lab is supported by the Francis Crick Institute, which receives its core funding from Cancer Research UK (FC001175), the UK Medical Research Council (FC001175), and the Wellcome Trust (FC001175). This research was funded in part by the Wellcome Trust (FC001175). For the purpose of Open Access, the author has applied a CC BY public copyright license to any Author Accepted Manuscript version arising from this submission.

Author contributions

Conceptualization: E.C., N.T.; Software: D.B.; Formal analysis: E.C., M.H., D.B., A.W.; Investigation: E.C., Y.Z., B.A., M.H., A.W.; Writing – original draft preparation: All authors; Writing – review and editing: All authors; Supervision: E.C., N.T.; Funding acquisition: E.C., N.T.

References

Aguilar-Aragon, M., Fletcher, G. and Thompson, B. J. (2020). The cytoskeletal motor proteins Dynein and MyoV direct apical transport of Crumbs. *Dev Biol* **459**, 126-137.

Ahmed, S. M. and Macara, I. G. (2017). The Par3 polarity protein is an exocyst receptor essential for mammary cell survival. *Nat Commun* **8**, 14867.

Ahmed, S. M., Nishida-Fukuda, H., Li, Y., McDonald, W. H., Gradinaru, C. C. and Macara, I. G. (2018). Exocyst dynamics during vesicle tethering and fusion. *Nat Commun* **9**, 5140.

Aigouy, B., Farhadifar, R., Staple, D. B., Sagner, A., Roper, J. C., Julicher, F. and Eaton, S. (2010). Cell flow reorients the axis of planar polarity in the wing epithelium of Drosophila. *Cell* **142**, 773-86.

Bai, J., Chiu, W., Wang, J., Tzeng, T., Perrimon, N. and Hsu, J. (2001). The cell adhesion molecule Echinoid defines a new pathway that antagonizes the Drosophila EGF receptor signaling pathway. *Development* **128**, 591-601.

Banerjee, J. J., Aerne, B. L., Holder, M. V., Hauri, S., Gstaiger, M. and Tapon, N. (2017). Meru couples planar cell polarity with apical-basal polarity during asymmetric cell division. *Elife* **6**.

Bardet, P. L., Guirao, B., Paoletti, C., Serman, F., Leopold, V., Bosveld, F., Goya, Y., Mirouse, V., Graner, F. and Bellaiche, Y. (2013). PTEN controls junction lengthening and stability during cell rearrangement in epithelial tissue. *Dev Cell* **25**, 534-46.

Beronja, S., Laprise, P., Papoulas, O., Pellikka, M., Sisson, J. and Tepass, U. (2005). Essential function of Drosophila Sec6 in apical exocytosis of epithelial photoreceptor cells. *J Cell Biol* **169**, 635-46.

Blankenship, J. T., Fuller, M. T. and Zallen, J. A. (2007). The Drosophila homolog of the Exo84 exocyst subunit promotes apical epithelial identity. *J Cell Sci* **120**, 3099-110.

Bour, B. A., Chakravarti, M., West, J. M. and Abmayr, S. M. (2000). Drosophila SNS, a member of the immunoglobulin superfamily that is essential for myoblast fusion. *Genes Dev* **14**, 1498-511.

Boyd, C., Hughes, T., Pypaert, M. and Novick, P. (2004). Vesicles carry most exocyst subunits to exocytic sites marked by the remaining two subunits, Sec3p and Exo70p. *J Cell Biol* **167**, 889-901.

Bryant, D. M., Datta, A., Rodriguez-Fraticelli, A. E., Peranen, J., Martin-Belmonte, F. and Mostov, K. E. (2010). A molecular network for de novo generation of the apical surface and lumen. *Nat Cell Biol* **12**, 1035-45.

Campbell, K., Knust, E. and Skaer, H. (2009). Crumbs stabilises epithelial polarity during tissue remodelling. *J Cell Sci* **122**, 2604-12.

Chandra, S., Ahmed, A. and Vaessin, H. (2003). The Drosophila IgC2 domain protein friend-of-echinoid, a paralogue of echinoid, limits the number of sensory organ precursors in the wing disc and interacts with the Notch signaling pathway. *Developmental Biology* **256**, 302-316.

Chang, L. H., Chen, P., Lien, M. T., Ho, Y. H., Lin, C. M., Pan, Y. T., Wei, S. Y. and Hsu, J. C. (2011). Differential adhesion and actomyosin cable collaborate to drive Echinoid-mediated cell sorting. *Development* **138**, 3803-12.

Charras, G. and Yap, A. S. (2018). Tensile Forces and Mechanotransduction at Cell–Cell Junctions. *Current Biology* **28**, R445-R457.

Classen, A. K., Anderson, K. I., Marois, E. and Eaton, S. (2005). Hexagonal packing of Drosophila wing epithelial cells by the planar cell polarity pathway. *Dev Cell* **9**, 805-17.

Cong, W., Hirose, T., Harita, Y., Yamashita, A., Mizuno, K., Hirano, H. and Ohno, S. (2010). ASPP2 regulates epithelial cell polarity through the PAR complex. *Curr Biol* **20**, 1408-14.

Das, A., Gajendra, S., Falenta, K., Oudin, M. J., Peschard, P., Feng, S., Wu, B., Marshall, C. J., Doherty, P., Guo, W. et al. (2014). RalA promotes a direct exocyst-Par6 interaction to regulate polarity in neuronal development. *J Cell Sci* **127**, 686-99.

Diaz de la Loza, M. C. and Thompson, B. J. (2017). Forces shaping the Drosophila wing. *Mech Dev* **144**, 23-32.

Diaz-de-la-Loza, M. D., Ray, R. P., Ganguly, P. S., Alt, S., Davis, J. R., Hoppe, A., Tapon, N., Salbreux, G. and Thompson, B. J. (2018). Apical and Basal Matrix Remodeling Control Epithelial Morphogenesis. *Dev Cell* **46**, 23-39 e5.

Eaton, S. and Julicher, F. (2011). Cell flow and tissue polarity patterns. *Curr Opin Genet Dev* **21**, 747-52.

Eberl, D. F. and Hilliker, A. J. (1988). Characterization of X-linked recessive lethal mutations affecting embryonic morphogenesis in Drosophila melanogaster. *Genetics* **118**, 109-20.

Escudero, L. M., Wei, S. Y., Chiu, W. H., Modolell, J. and Hsu, J. C. (2003). Echinoid synergizes with the Notch signaling pathway in Drosophila mesothorax bristle patterning. *Development* **130**, 6305-16.

Etournay, R., Merkel, M., Popovic, M., Brandl, H., Dye, N. A., Aigouy, B., Salbreux, G., Eaton, S. and Julicher, F. (2016). TissueMiner: A multiscale analysis toolkit to quantify how cellular processes create tissue dynamics. *Elife* **5**.

Etournay, R., Popovic, M., Merkel, M., Nandi, A., Blasse, C., Aigouy, B., Brandl, H., Myers, G., Salbreux, G., Julicher, F. et al. (2015). Interplay of cell dynamics and epithelial tension during morphogenesis of the Drosophila pupal wing. *Elife* **4**, e07090.

Fetting, J. L., Spencer, S. A. and Wolff, T. (2009). The cell adhesion molecules Echinoid and Friend of Echinoid coordinate cell adhesion and cell signaling to regulate the fidelity of ommatidial rotation in the Drosophila eye. *Development* **136**, 3323-33.

Galletta, B. J., Chakravarti, M., Banerjee, R. and Abmayr, S. M. (2004). SNS: Adhesive properties, localization requirements and ectodomain dependence in S2 cells and embryonic myoblasts. *Mech Dev* **121**, 1455-68.

Ganesan, S. J., Feyder, M. J., Chemmama, I. E., Fang, F., Rout, M. P., Chait, B. T., Shi, Y., Munson, M. and Sali, A. (2020). Integrative structure and function of the yeast exocyst complex. *Protein Sci* **29**, 1486-1501.

Gault, W. J., Olguin, P., Weber, U. and Mlodzik, M. (2012). Drosophila CK1-gamma, gilgamesh, controls PCP-mediated morphogenesis through regulation of vesicle trafficking. *J Cell Biol* **196**, 605-21.

Grindstaff, K. K., Yeaman, C., Anandasabapathy, N., Hsu, S. C., Rodriguez-Boulan, E., Scheller, R. H. and Nelson, W. J. (1998). Sec6/8 complex is recruited to cell-cell contacts and specifies transport vesicle delivery to the basal-lateral membrane in epithelial cells. *Cell* **93**, 731-40.

Guirao, B., Rigaud, S. U., Bosveld, F., Bailles, A., Lopez-Gay, J., Ishihara, S., Sugimura, K., Graner, F. and Bellaiche, Y. (2015). Unified quantitative characterization of epithelial tissue development. *Elife* **4**.

Harris, T. J. and Tepass, U. (2010). Adherens junctions: from molecules to morphogenesis. *Nat Rev Mol Cell Biol* **11**, 502-14.

He, B., Xi, F., Zhang, X., Zhang, J. and Guo, W. (2007). Exo70 interacts with phospholipids and mediates the targeting of the exocyst to the plasma membrane. *EMBO J* **26**, 4053-65.

Heider, M. R., Gu, M., Duffy, C. M., Mirza, A. M., Marcotte, L. L., Walls, A. C., Farrall, N., Hakhverdyan, Z., Field, M. C., Rout, M. P. et al. (2016). Subunit connectivity, assembly determinants and architecture of the yeast exocyst complex. *Nat Struct Mol Biol* **23**, 59-66.

Heider, M. R. and Munson, M. (2012). Exorcising the exocyst complex. *Traffic* **13**, 898-907.

Held, L. I. (2002). Imaginal discs : the genetic and cellular logic of pattern formation. Cambridge ; New York: Cambridge University Press.

Ho, Y. H., Lien, M. T., Lin, C. M., Wei, S. Y., Chang, L. H. and Hsu, J. C. (2010). Echinoid regulates Flamingo endocytosis to control ommatidial rotation in the Drosophila eye. *Development* **137**, 745-54.

Huang, J., Zhou, W., Dong, W., Watson, A. M. and Hong, Y. (2009). From the Cover: Directed, efficient, and versatile modifications of the Drosophila genome by genomic engineering. *Proc Natl Acad Sci U S A* **106**, 8284-9.

Islam, R., Wei, S. Y., Chiu, W. H., Hortsch, M. and Hsu, J. C. (2003). Neuroglian activates Echinoid to antagonize the Drosophila EGF receptor signaling pathway. *Development* **130**, 2051-9.

Jafar-Nejad, H., Andrews, H. K., Acar, M., Bayat, V., Wirtz-Peitz, F., Mehta, S. Q., Knoblich, J. A. and Bellen, H. J. (2005). Sec15, a component of the exocyst, promotes notch signaling during the asymmetric division of Drosophila sensory organ precursors. *Dev Cell* **9**, 351-63.

Lalli, G. (2009). RalA and the exocyst complex influence neuronal polarity through PAR-3 and aPKC. *J Cell Sci* **122**, 1499-506.

Langevin, J., Morgan, M. J., Sibarita, J. B., Aresta, S., Murthy, M., Schwarz, T., Camonis, J. and Bellaiche, Y. (2005). Drosophila exocyst components Sec5, Sec6, and Sec15 regulate DE-Cadherin trafficking from recycling endosomes to the plasma membrane. *Dev Cell* **9**, 365-76.

Langton, P. F., Colombani, J., Aerne, B. L. and Tapon, N. (2007). Drosophila ASPP regulates C-terminal Src kinase activity. *Dev Cell* **13**, 773-82.

Langton, P. F., Colombani, J., Chan, E. H., Wepf, A., Gstaiger, M. and Tapon, N. (2009). The dASPP-dRASSF8 complex regulates cell-cell adhesion during Drosophila retinal morphogenesis. *Curr Biol* **19**, 1969-78.

Laplante, C. and Nilson, L. A. (2006). Differential expression of the adhesion molecule Echinoid drives epithelial morphogenesis in Drosophila. *Development* **133**, 3255-64.

Legland, D., Arganda-Carreras, I. and Andrey, P. (2016). MorphoLibJ: integrated library and plugins for mathematical morphology with ImageJ. *Bioinformatics* **32**, 3532-3534.

Li, Y. C., Yang, W. T., Cheng, L. C., Lin, C. M., Ho, Y. H., Lin, P. Y., Chen, B. C., Rickoll, W. L. and Hsu, J. C. (2015). Novel transport function of adherens junction revealed by live imaging in Drosophila. *Biochem Biophys Res Commun* **463**, 686-92.

Lin, H. P., Chen, H. M., Wei, S. Y., Chen, L. Y., Chang, L. H., Sun, Y. J., Huang, S. Y. and Hsu, J. C. (2007). Cell adhesion molecule Echinoid associates with unconventional myosin VI/Jaguar motor to regulate cell morphology during dorsal closure in Drosophila. *Dev Biol* **311**, 423-33.

Lipschutz, J. H. (2019). The role of the exocyst in renal ciliogenesis, cystogenesis, tubulogenesis, and development. *Kidney Res Clin Pract* **38**, 260-266.

Lipschutz, J. H., Guo, W., O'Brien, L. E., Nguyen, Y. H., Novick, P. and Mostov, K. E. (2000). Exocyst is involved in cystogenesis and tubulogenesis and acts by modulating synthesis and delivery of basolateral plasma membrane and secretory proteins. *Mol Biol Cell* **11**, 4259-75.

Liu, D., Li, X., Shen, D. and Novick, P. (2018). Two subunits of the exocyst, Sec3p and Exo70p, can function exclusively on the plasma membrane. *Mol Biol Cell* **29**, 736-750.

Liu, J., Zuo, X., Yue, P. and Guo, W. (2007). Phosphatidylinositol 4,5-bisphosphate mediates the targeting of the exocyst to the plasma membrane for exocytosis in mammalian cells. *Mol Biol Cell* **18**, 4483-92.

Lloyd, T. E., Atkinson, R., Wu, M. N., Zhou, Y., Pennetta, G. and Bellen, H. J. (2002). Hrs Regulates Endosome Membrane Invagination and Tyrosine Kinase Receptor Signaling in Drosophila. *Cell* **108**, 261-269.

Ma, D., Amonlirdviman, K., Raffard, R. L., Abate, A., Tomlin, C. J. and Axelrod, J. D. (2008). Cell packing influences planar cell polarity signaling. *Proc Natl Acad Sci U S A* **105**, 18800-5.

Mandai, K., Rikitake, Y., Shimono, Y. and Takai, Y. (2013). Afadin/AF-6 and canoe: roles in cell adhesion and beyond. *Prog Mol Biol Transl Sci* **116**, 433-54.

Mao, Q. and Lecuit, T. (2016). Mechanochemical Interplay Drives Polarization in Cellular and Developmental Systems. *Curr Top Dev Biol* **116**, 633-57.

Mateus, A. M., Gorfinkiel, N., Schamberg, S. and Martinez Arias, A. (2011). Endocytic and recycling endosomes modulate cell shape changes and tissue behaviour during morphogenesis in Drosophila. *PLoS One* **6**, e18729.

Mehta, S. Q., Hiesinger, P. R., Beronja, S., Zhai, R. G., Schulze, K. L., Verstreken, P., Cao, Y., Zhou, Y., Tepass, U., Crair, M. C. et al. (2005). Mutations in Drosophila sec15 reveal a function in neuronal targeting for a subset of exocyst components. *Neuron* **46**, 219-32.

Mei, K., Li, Y., Wang, S., Shao, G., Wang, J., Ding, Y., Luo, G., Yue, P., Liu, J. J., Wang, X. et al. (2018). Cryo-EM structure of the exocyst complex. *Nat Struct Mol Biol* **25**, 139-146.

Murthy, M., Garza, D., Scheller, R. H. and Schwarz, T. L. (2003). Mutations in the exocyst component Sec5 disrupt neuronal membrane traffic, but neurotransmitter release persists. *Neuron* **37**, 433-47.

Murthy, M., Ranjan, R., Denef, N., Higashi, M. E., Schupbach, T. and Schwarz, T. L. (2005). Sec6 mutations and the Drosophila exocyst complex. *J Cell Sci* **118**, 1139-50.

Ozkan, E., Carrillo, R. A., Eastman, C. L., Weiszmann, R., Waghray, D., Johnson, K. G., Zinn, K., Celniker, S. E. and Garcia, K. C. (2013). An extracellular interactome of immunoglobulin and LRR proteins reveals receptor-ligand networks. *Cell* **154**, 228-39.

Oztan, A., Silvis, M., Weisz, O. A., Bradbury, N. A., Hsu, S. C., Goldenring, J. R., Yeaman, C. and Apodaca, G. (2007). Exocyst requirement for endocytic traffic directed toward the apical and basolateral poles of polarized MDCK cells. *Mol Biol Cell* **18**, 3978-92.

Pare, A. C. and Zallen, J. A. (2020). Cellular, molecular, and biophysical control of epithelial cell intercalation. *Curr Top Dev Biol* **136**, 167-193.

Perez-Vale, K. Z. and Peifer, M. (2020). Orchestrating morphogenesis: building the body plan by cell shape changes and movements. *Development* **147**.

Pleskot, R., Cwiklik, L., Jungwirth, P., Zarsky, V. and Potocky, M. (2015). Membrane targeting of the yeast exocyst complex. *Biochim Biophys Acta* **1848**, 1481-9.

Polgar, N. and Fogelgren, B. (2018). Regulation of Cell Polarity by Exocyst-Mediated Trafficking. *Cold Spring Harb Perspect Biol* **10**.

Ponting, C. P. and Benjamin, D. R. (1996). A novel family of Ras-binding domains. *Trends Biochem Sci* **21**, 422-5.

Rawlins, E. L., Lovegrove, B. and Jarman, A. P. (2003a). Echinoid facilitates Notch pathway signalling during Drosophila neurogenesis through functional interaction with Delta. *Development* **130**, 6475-84.

Rawlins, E. L., White, N. M. and Jarman, A. P. (2003b). Echinoid limits R8 photoreceptor specification by inhibiting inappropriate EGF receptor signalling within R8 equivalence groups. *Development* **130**, 3715-24.

Ray, R. P., Matamoro-Vidal, A., Ribeiro, P. S., Tapon, N., Houle, D., Salazar-Ciudad, I. and Thompson, B. J. (2015). Patterned Anchorage to the Apical Extracellular Matrix Defines Tissue Shape in the Developing Appendages of Drosophila. *Dev Cell* **34**, 310-22.

Ribeiro, P. S., Josue, F., Wepf, A., Wehr, M. C., Rinner, O., Kelly, G., Tapon, N. and Gstaiger, M. (2010). Combined functional genomic and proteomic approaches identify a PP2A complex as a negative regulator of Hippo signaling. *Mol Cell* **39**, 521-34.

Roeth, J. F., Sawyer, J. K., Wilner, D. A. and Peifer, M. (2009). Rab11 helps maintain apical crumbs and adherens junctions in the Drosophila embryonic ectoderm. *PLoS One* **4**, e7634.

Roman-Fernandez, A. and Bryant, D. M. (2016). Complex Polarity: Building Multicellular Tissues Through Apical Membrane Traffic. *Traffic* **17**, 1244-1261.

Rusu, A. D. and Georgiou, M. (2020). The multifarious regulation of the apical junctional complex. *Open Biol* **10**, 190278.

Satoh, A. K., O'Tousa, J. E., Ozaki, K. and Ready, D. F. (2005). Rab11 mediates post-Golgi trafficking of rhodopsin to the photosensitive apical membrane of Drosophila photoreceptors. *Development* **132**, 1487-97.

Schneider, T., Reiter, C., Eule, E., Bader, B., Lichte, B., Nie, Z., Schimansky, T., Ramos, R. G. P. and Fischbach, K.-F. (1995). Restricted expression of the irreC-rst protein is required for normal axonal projections of columnar visual neurons. *Neuron* **15**, 259-271.

Sottocornola, R., Royer, C., Vives, V., Tordella, L., Zhong, S., Wang, Y., Ratnayaka, I., Shipman, M., Cheung, A., Gaston-Massuet, C. et al. (2010). ASPP2 binds Par-3 and controls the polarity and proliferation of neural progenitors during CNS development. *Dev Cell* **19**, 126-37.

Spencer, S. A. and Cagan, R. L. (2003). Echinoid is essential for regulation of Egfr signaling and R8 formation during Drosophila eye development. *Development* **130**, 3725-33.

Strutt, H. and Strutt, D. (2002). Nonautonomous Planar Polarity Patterning in Drosophila. *Dev Cell* **3**, 851-863.

Sugie, A., Umetsu, D., Yasugi, T., Fischbach, K. F. and Tabata, T. (2010). Recognition of pre- and postsynaptic neurons via nephrin/NEPH1 homologs is a basis for the formation of the Drosophila retinotopic map. *Development* **137**, 3303-13.

Tanaka, T. and Nakamura, A. (2008). The endocytic pathway acts downstream of Oskar in Drosophila germ plasm assembly. *Development* **135**, 1107-17.

TerBush, D. R., Maurice, T., Roth, D. and Novick, P. (1996). The Exocyst is a multiprotein complex required for exocytosis in Saccharomyces cerevisiae. *EMBO J* **15**, 6483-94.

TerBush, D. R. and Novick, P. (1995). Sec6, Sec8, and Sec15 are components of a multisubunit complex which localizes to small bud tips in Saccharomyces cerevisiae. *J Cell Biol* **130**, 299-312.

van Leen, E. V., di Pietro, F. and Bellaiche, Y. (2020). Oriented cell divisions in epithelia: from force generation to force anisotropy by tension, shape and vertices. *Curr Opin Cell Biol* **62**, 9-16.

Walther, R. F., Nunes de Almeida, F., Vlassaks, E., Burden, J. J. and Pichaud, F. (2016). Pak4 Is Required during Epithelial Polarity Remodeling through Regulating AJ Stability and Bazooka Retention at the ZA. *Cell Rep* **15**, 45-53.

Wanaguru, M., Barry, D. J., Benton, D. J., O'Reilly, N. J. and Bishop, K. N. (2018). Murine leukemia virus p12 tethers the capsid-containing pre-integration complex to chromatin by binding directly to host nucleosomes in mitosis. *PLoS Pathog* **14**, e1007117.

Warrington, S. J., Strutt, H. and Strutt, D. (2013). The Frizzled-dependent planar polarity pathway locally promotes E-cadherin turnover via recruitment of RhoGEF2. *Development*.

Wei, S. Y., Escudero, L. M., Yu, F., Chang, L. H., Chen, L. Y., Ho, Y. H., Lin, C. M., Chou, C. S., Chia, W., Modolell, J. et al. (2005). Echinoid is a component of adherens junctions that cooperates with DE-Cadherin to mediate cell adhesion. *Dev Cell* **8**, 493-504.

Wu, S., Mehta, S. Q., Pichaud, F., Bellen, H. J. and Quiocho, F. A. (2005). Sec15 interacts with Rab11 via a novel domain and affects Rab11 localization in vivo. *Nat Struct Mol Biol* **12**, 879-85.

Xiong, X., Xu, Q., Huang, Y., Singh, R. D., Anderson, R., Leof, E., Hu, J. and Ling, K. (2012). An association between type Igamma PI4P 5-kinase and Exo70 directs E-cadherin clustering and epithelial polarization. *Mol Biol Cell* **23**, 87-98.

Yeaman, C., Grindstaff, K. K. and Nelson, W. J. (2004). Mechanism of recruiting Sec6/8 (exocyst) complex to the apical junctional complex during polarization of epithelial cells. *J Cell Sci* **117**, 559-70.

Yue, T., Tian, A. and Jiang, J. (2012). The cell adhesion molecule echinoid functions as a tumor suppressor and upstream regulator of the Hippo signaling pathway. *Dev Cell* **22**, 255-67.

Zaessinger, S., Zhou, Y., Bray, S. J., Tapon, N. and Djiane, A. (2015). Drosophila MAGI interacts with RASSF8 to regulate E-Cadherin-based adherens junctions in the developing eye. *Development* **142**, 1102-12.

Zago, G., Biondini, M., Camonis, J. and Parrini, M. C. (2019). A family affair: A Ral-exocyst-centered network links Ras, Rac, Rho signaling to control cell migration. *Small GTPases* **10**, 323-330.

Zeng, J., Feng, S., Wu, B. and Guo, W. (2017). Polarized Exocytosis. *Cold Spring Harb Perspect Biol* **9**.

Zhang, X., Orlando, K., He, B., Xi, F., Zhang, J., Zajac, A. and Guo, W. (2008). Membrane association and functional regulation of Sec3 by phospholipids and Cdc42. *J Cell Biol* **180**, 145-58.

Zhang, X. M., Ellis, S., Sriratana, A., Mitchell, C. A. and Rowe, T. (2004). Sec15 is an effector for the Rab11 GTPase in mammalian cells. *J Biol Chem* **279**, 43027-34.

Zuo, X., Fogelgren, B. and Lipschutz, J. H. (2011). The small GTPase Cdc42 is necessary for primary ciliogenesis in renal tubular epithelial cells. *J Biol Chem* **286**, 22469-77.

FIGURES

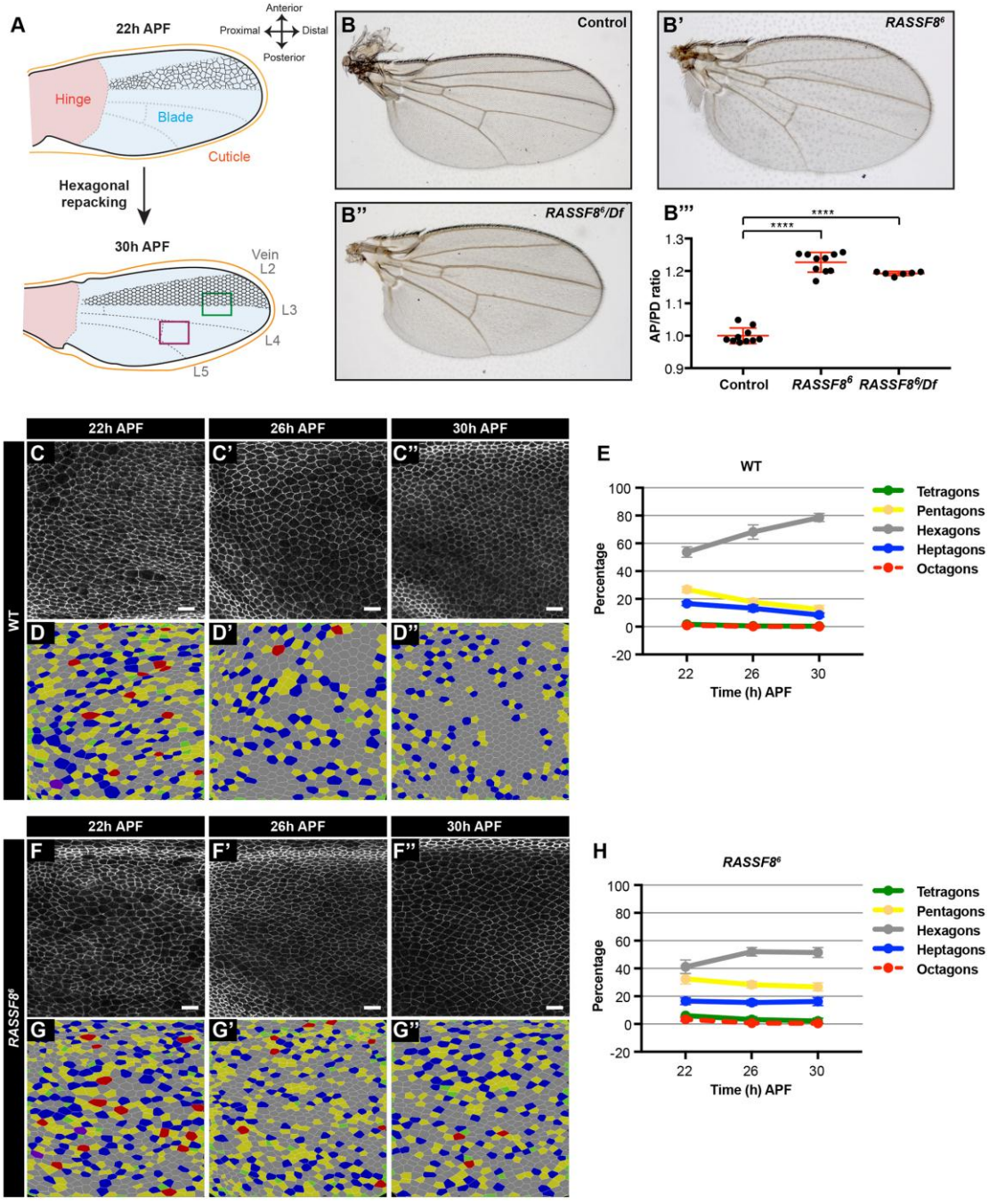

Fig. 1. RASSF8 is required for pupal wing cell hexagonal packing

(A) Schematic diagram of pupal wing morphology, axes and development from 22 to 30 hours after puparium formation (APF). Colour-coded rectangles indicate regions imaged for analyses. The positions of the longitudinal veins (L2-L5) and crossveins are indicated as dashed lines. As the wing hinge (shaded pink) contracts, the wing

blade (shaded blue) extends in the PD axis and the wing epithelial cells (indicated in black between L2 and L3) reorder to form a hexagonal lattice. The wing images throughout the manuscript are oriented as indicated in this diagram. (B) Wild type wing (B') *RASSF8*^{6} homozygous mutant wing (B'') *RASSF8*^{6}*/Df (3R)BSC321* deficiency heterozygous wing. (B''') Quantification of relative wing roundness (ratio of AP to PD axis, normalised so that wild type ratio = 1). Error bars = s.d.; ANOVA (Tukey's correction): ****p<0.0001. As expected since *RASSF8*^{6} is a null mutant, the homozygous *RASSF8*^{6} animals present a similar phenotype to the *RASSF8*^{6}/Df animals. (C-F) Hexagonal cell packing of wild type and *RASSF8* mutant wings at 22, 26, 30 hours APF. Images of Ecad::GFP labelled wild type (C-C") and *RASSF8* mutant (F-F") wings at a region distal to the posterior crossvein (purple rectangle in (A)). Colour-coded images indicate the number of neighbours for each cell in wild type (D-D") and *RASSF8* mutant (G-G") wings, determined by using Tissue Analyzer. (E, H) Percentage of cells with four, five, six, seven, eight neighbours (colour coded as indicated) in wild type (D) and *RASSF8* mutants (G). The red line (octagons) has been dashed so the green line (tetragons) can be seen. Error bar = s.d., n=1500-5000 cells from 3 to 5 individual wings. Scale bars: 10 µm. See Table S1 for raw data.

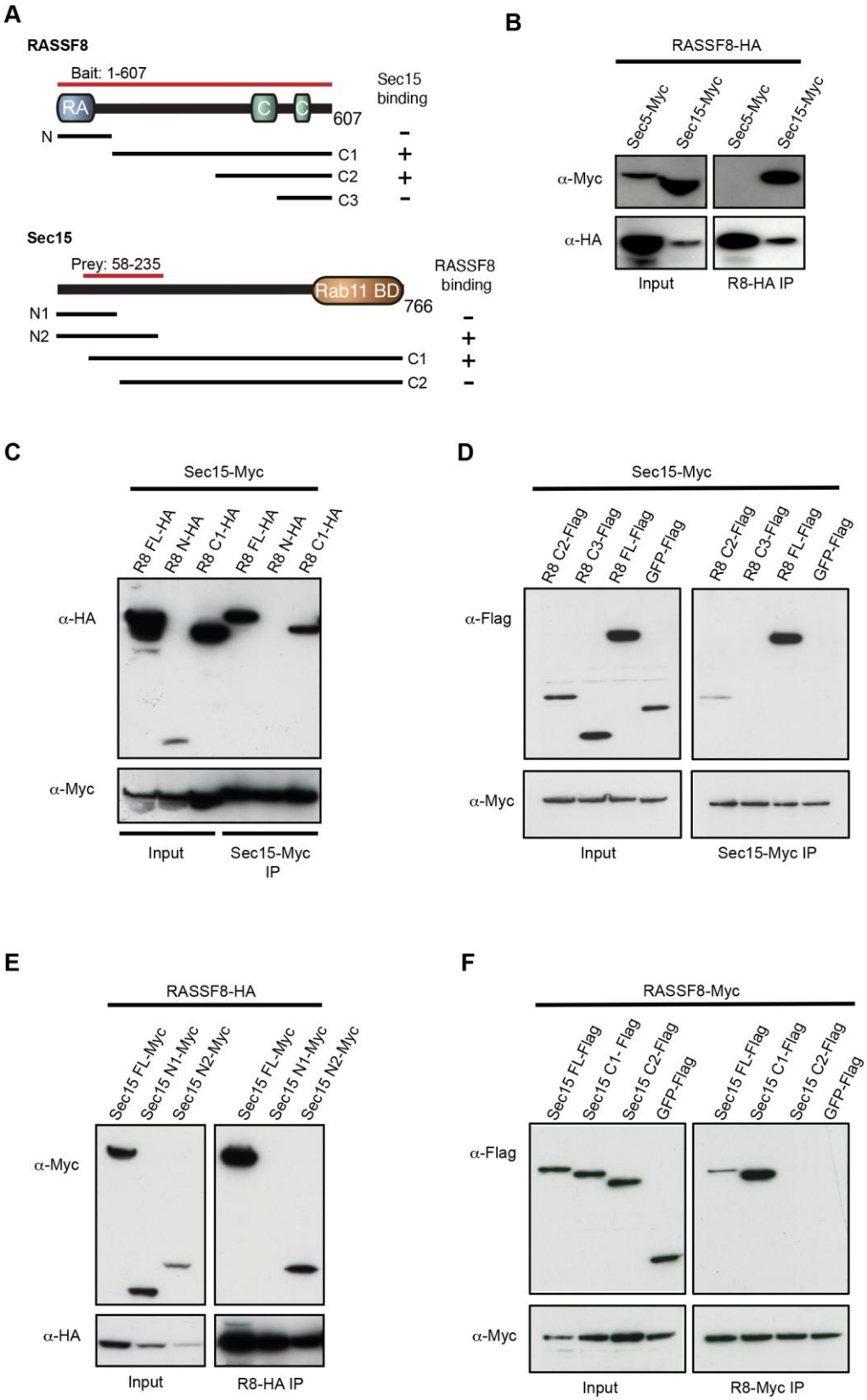

Fig. 2. Identification of Sec15 as a RASSF8 partner

(A) Schematic diagram of the RASSF8 and Sec15 proteins. The two-hybrid bait and prey, and the constructs used in the co-IP experiments are also shown (RASSF8: N, amino acids (a.a.) 1-120, C1, a.a. 121-607, C2, a.a. 350-607 and C3 a.a. 490-607; Sec15 N1, a.a. 1-134, N2, a.a. 1-225, C1, a.a. 58-766, C2, a.a. 130-766). (B-F) Co-IP experiment in S2 cells overexpressing the indicated constructs. (B) RASSF8-HA binds specifically to Sec15-Myc but not Sec5-Myc. (C, D) Amino acids 350-490 of RASSF8 are necessary for Sec15 binding. (E, F) Amino acids 135-225 of Sec15 are required for its interaction with RASSF8.

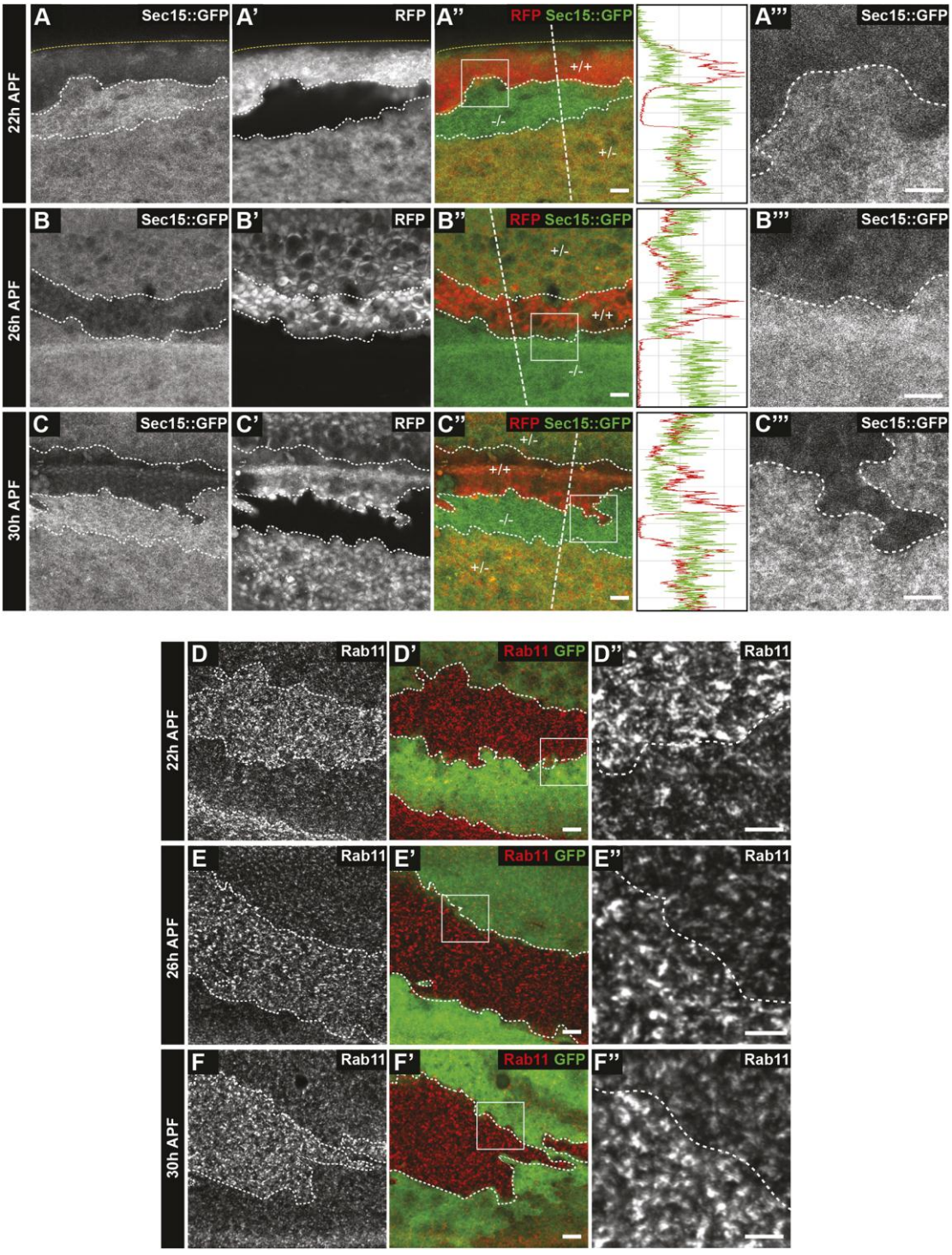

Fig. 3. Accumulation of Sec15 and Rab11 in *RASSF8* mutant pupal wing clones

(A-C''') Increase in Sec15::GFP (driven by the *ubiquitin* promoter) in *RASSF8* mutant clones (negative for RFP in red) at 22 (A-A''), 26 (B-B'') and 30 (C-C'') hours APF. Clone boundaries are marked by white dotted line. Yellow dotted line at 22 hours AFP shows the edge of the wing. In the merge channel, the genotypes of the clones

are given (+/+ wild type – two copies of RFP, +/- heterozygous – one copy of RFP, -/- homozygous *RASSF8* mutant – no copies of RFP). A’’’, B’’’ and C’’’ are zoomed-in view of the image in A”, B” and C” respectively marked by white boxes. Second last right panel shows the intensity profiles at the white dotted line in the merged image using Fiji. (D-F’’) Accumulation of Rab11 in *RASSF8* mutant clones. Rab11 antibody staining in *RASSF8* mutant clones marked by the absence of GFP at 22 (D-D’’), 26 (E-E’’), 30 (F-F’’) hours APF. D’’’, E’’’ and F’’’ are zoomed-in view of the image in D”, E” and F” respectively marked by white boxes. Scale bars: 10 µm except for zoomed-in panels (A’’’, B’’’, C’’’, D’’’, E’’’ and F’’’): 7 µm.

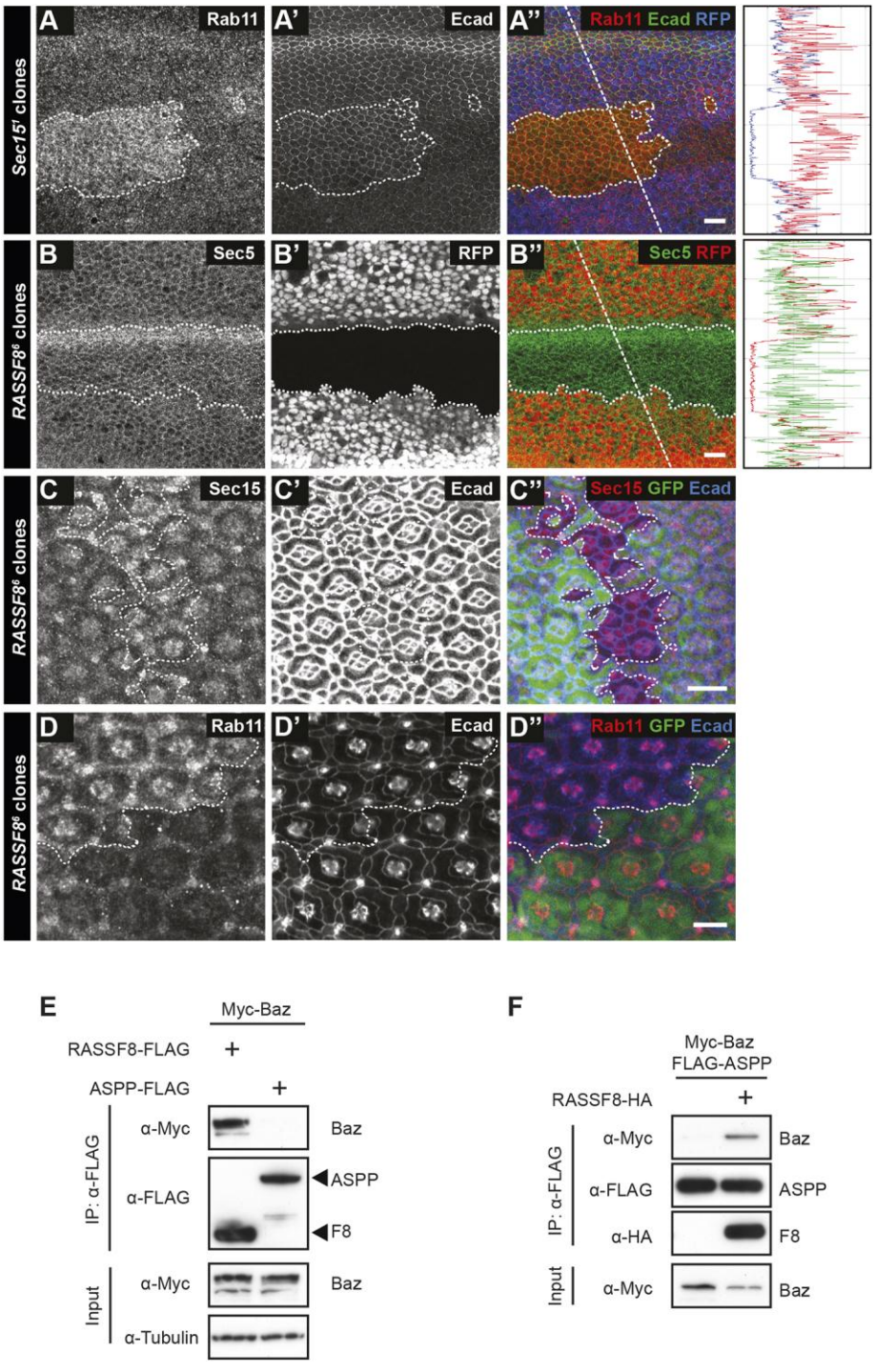

Fig. 4. Rab11 and Sec15, but not Sec5 are mislocalised in *RASSF8* mutant clones

(A-G'') Confocal micrographs of pupal wing discs and pupal retinas at 26 hours APF bearing *sec15* (A-A'') or *RASSF8* (B-G'') mutant clones generated using *hsFLP* (wing clones) or *eyFLP* (retinal clones) and stained as indicated. White dotted lines label the clone boundaries. (A-A'') Accumulation of Rab11 in *sec15* mutant clones marked by the absence of GFP in the pupal wing. (B-B'') Sec5 staining is not affected in

RASSF8 mutant pupal wing clones marked by the absence of GFP. Note that the horizontal line of elevated Sec5 intensity in the mutant clones corresponds to a wing vein. In (A-B''), the last right panel shows the intensity profiles at the white dotted line in the merged image using Fiji. (C-D'') Accumulation of Sec15 (C) and Rab11 (D) in *RASSF8* mutant clones marked by the absence of GFP in pupal retinas. Scale bars: 10 µm. (E, F) Co-IP experiment in S2 cells overexpressing the indicated constructs. (E) Baz associates with RASSF8 but not ASPP. (F) ASPP co-IPs Baz only in the presence of RASSF8.

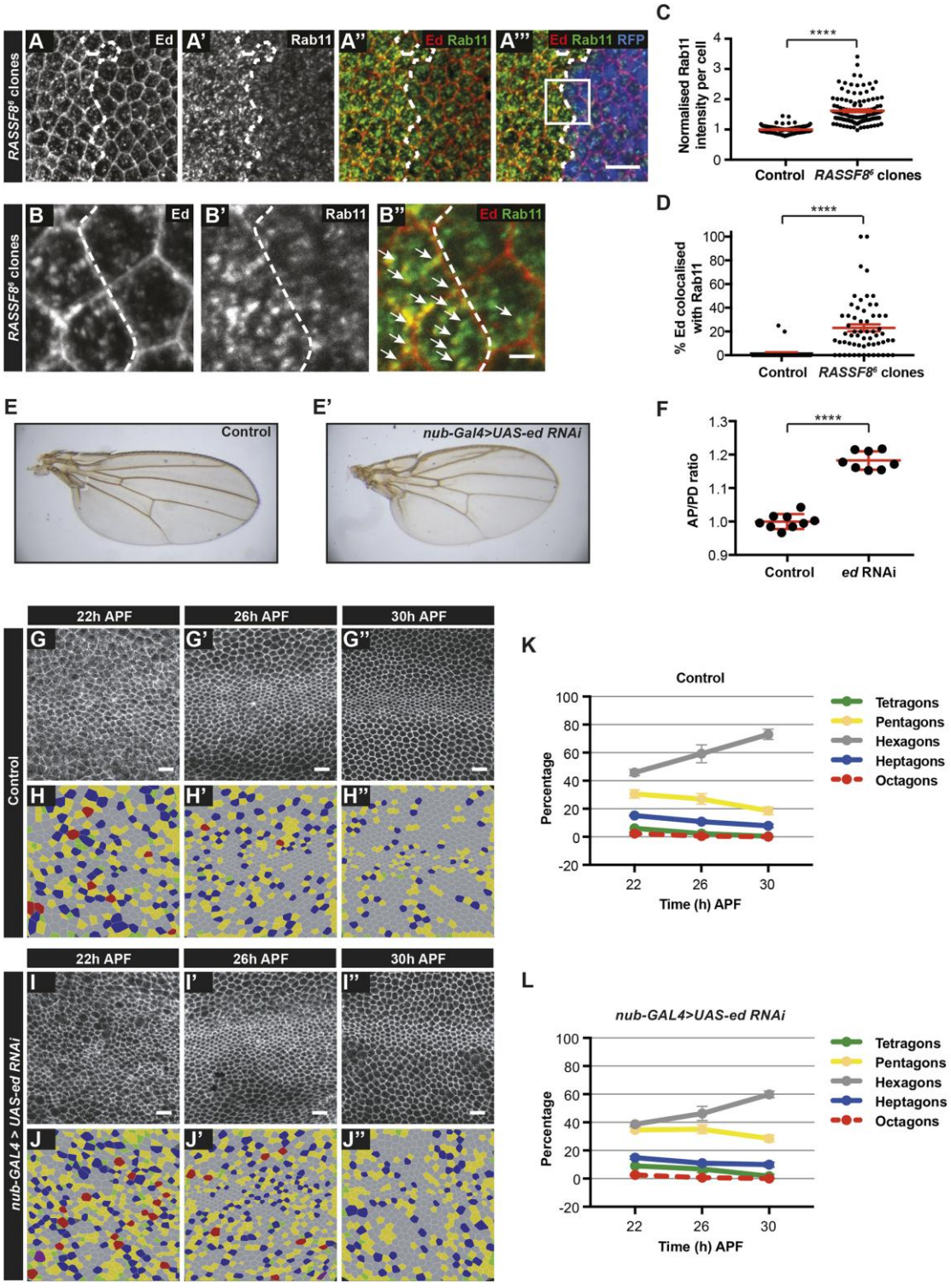

Fig. 5. Ed accumulates in Rab11 compartments in *RASSF8* mutants

(A-A'') Accumulation of Ed and Rab11 in *RASSF8* mutant clones. Ed (red) and Rab11 (green) antibody staining in *RASSF8* mutant clones (marked by absence of RFP in blue). Clone boundaries are marked by white dotted line. (B-B'') Zoomed-in view of the image in (A-A'''), see box in (A''') with colocalisation of Ed and Rab11 indicated

by white arrows. Note that Ed/Rab11-positive compartments are present both in the medial cytoplasm and at the apical plasma membrane. (C) Quantification of the total intracellular Rab11 fluorescence per cell in control (RFP+) or *RASSF8* mutant (RFP-) cells. The *RASSF8* mutant values were normalised to the control values. Error bars = s.e.m.; n>44 cells from 3 different wings. Two-tailed Student's t-test: **** p<0.0001. (D) Quantification of the percentage of Ed colocalised with Rab11 per cell in control (RFP+) or *RASSF8* mutant (RFP-) cells. Error bars = s.e.m.; n>34 cells from 3 different wings. Two-tailed Student's t-test: **** p<0.0001. (E) Control wing (E') *nub-Gal4* driven *UAS-ed-RNAi* wing (F) Quantification of relative wing roundness (ratio of AP to PD axis, normalised so that wild type ratio = 1). Error bars = s.d.; Two-tailed Student's t-test: ****p<0.0001. (G-L) Hexagonal cell packing of control and *nub-Gal4*-driven *ed-RNAi* wings at 22, 26, 30 hours after puparium formation (APF). Confocal images of a region straddling the L3 vein (green rectangle in Fig. 1A) of control (G-G'') and *ed-RNAi* (I-I'') pupal wings stained with anti-Arm antibodies. Colour-coded images indicate the number of neighbours for each cell in control (H-H'') and *ed-RNAi* (J-J''). (K, L) Percentage of cells with four, five, six, seven, eight neighbours (colour coded as indicated) in control (K) and *ed-RNAi* wings (L). The red line (octagons) has been dashed so the green line (tetragons) can be seen. Error bars = s.d.; n=1600-4600 cells from 4 to 8 individual wings. Scale bars in A, G and I: 10 µm, in B: 2 µm. See Table S2 for raw data.

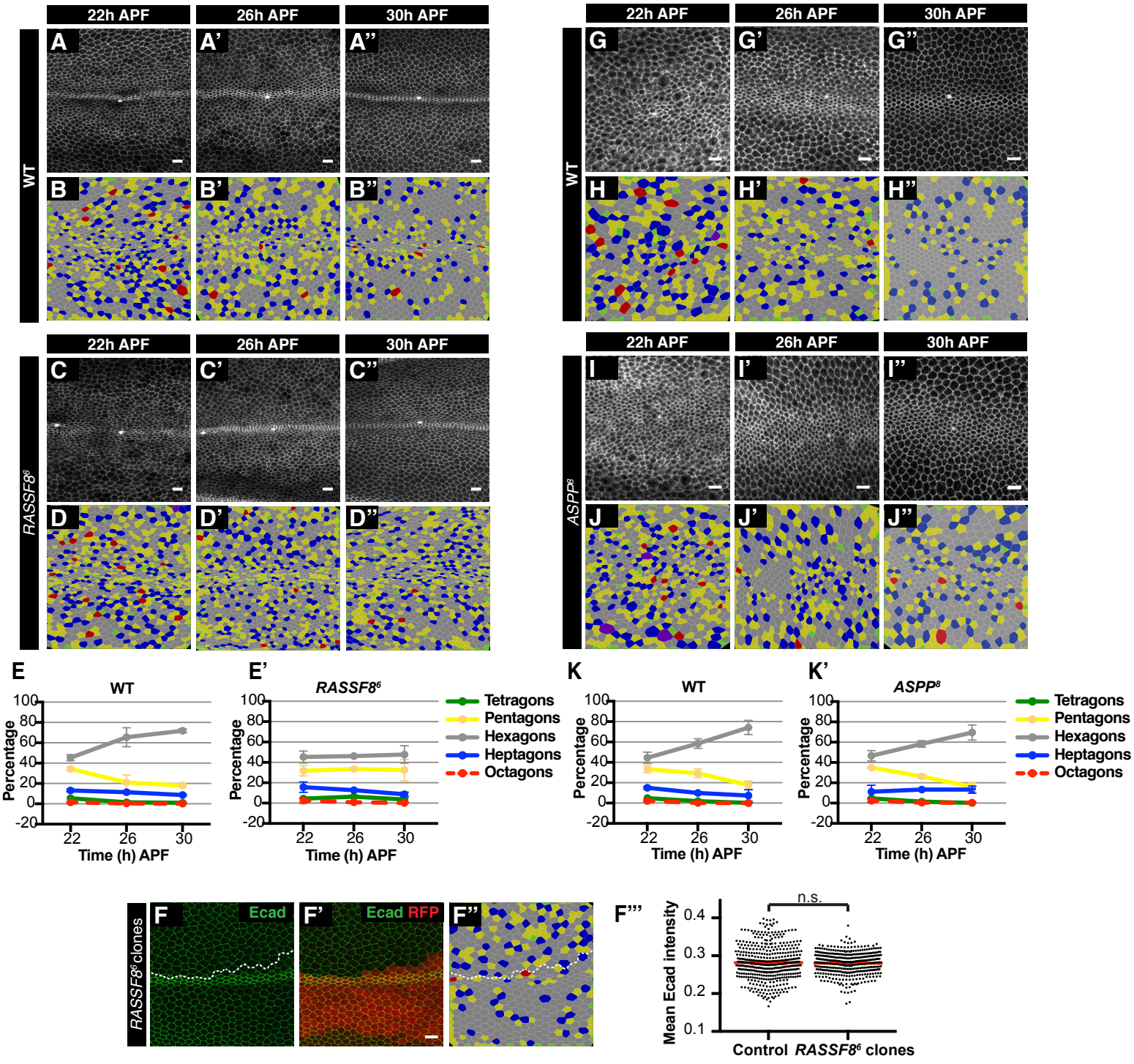

Fig. S1. Wing cell packing defects in *RASSF8* mutants

(A-D'') Confocal images of Ecad::GFP-labelled wild type (A) and *RASSF8* mutant (C) pupal wings in a region straddling the L3 vein (green rectangle in Fig. 1A) at 22, 26, 30 hours APF. Colour-coded images indicate the number of neighbours for each cell in wild type (B) and *RASSF8* mutant (D). (E-E') Percentage of cells with four, five, six, seven or eight neighbours (colour coded as indicated) in wild type (E) and *RASSF8* mutants (E') (n=2500-5000 cells from 3 to 5 individual wings; error bars = s.d.). (F-F'') *RASSF8* mutants alter hexagonal cell packing cell autonomously. Ecad::GFP and merged images of *RASSF8* mutant clones marked by the absence of RFP at 36 hours APF. Clone boundaries are marked by white dotted line. (F''') Quantification of average Ecad::GFP intensity per cell at the cell junctions in control and *RASSF8* mutant cells. Error bars = s.e.m.; n=415-451 cells from 3 different wings. Two-tailed Student's t-test: n.s.=not significant (p=0.67). (G-J'') Confocal images of Ecad::GFP-labelled wild type (G) and *ASPP* mutant (I) pupal wings in a region straddling the L3 vein (green rectangle in Fig. 1A) at 22, 26, 30 hours APF. Colour-coded images indicate the number of neighbours for each cell in wild type (H) and *ASPP* mutant (J). (K, K') Percentage of cells with four, five, six, seven or eight neighbours (colour coded as indicated) in wild type (K) and *ASPP* mutants (K'). The red line (octagons) has been dashed so the green line (tetragons) can be seen. n=1400-3000 cells from 3 to 8 individual wings; error bars = s.d. Scale bars: 10 µm. See Table S1 for raw data.

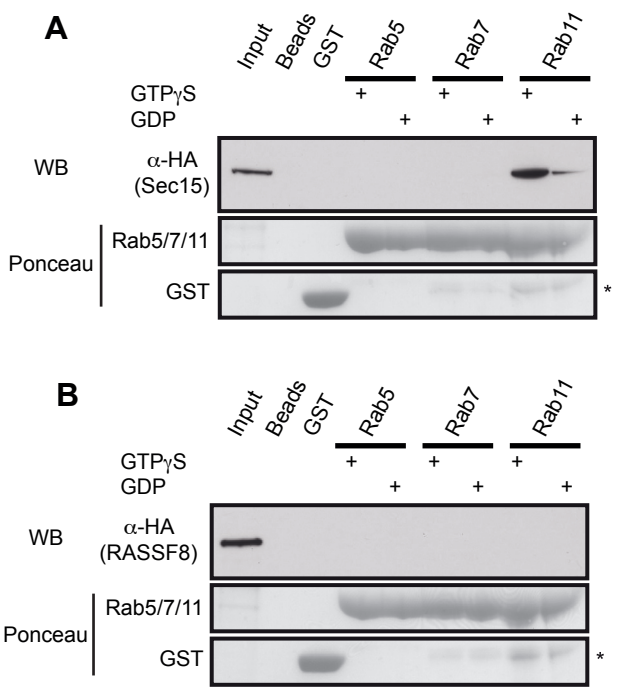

Fig. S2. RASSF8 does not directly bind to Rab11

(A, B) GST-pulldown experiments using GST-Rab5 (early endosomes), Rab7 (lysosomes) and Rab11 (recycling or biosynthetic endosomes) with (A) Sec15 or (B) RASSF8. Rab family GTPases were loaded with GTPγS or GDP. As controls, Glutathione beads and GST-only pulldowns were used. Equal protein levels of small GTPases and GST were verified by Ponceau S staining (middle and bottom panels). Asterisks mark degradation products of the small GTPases.

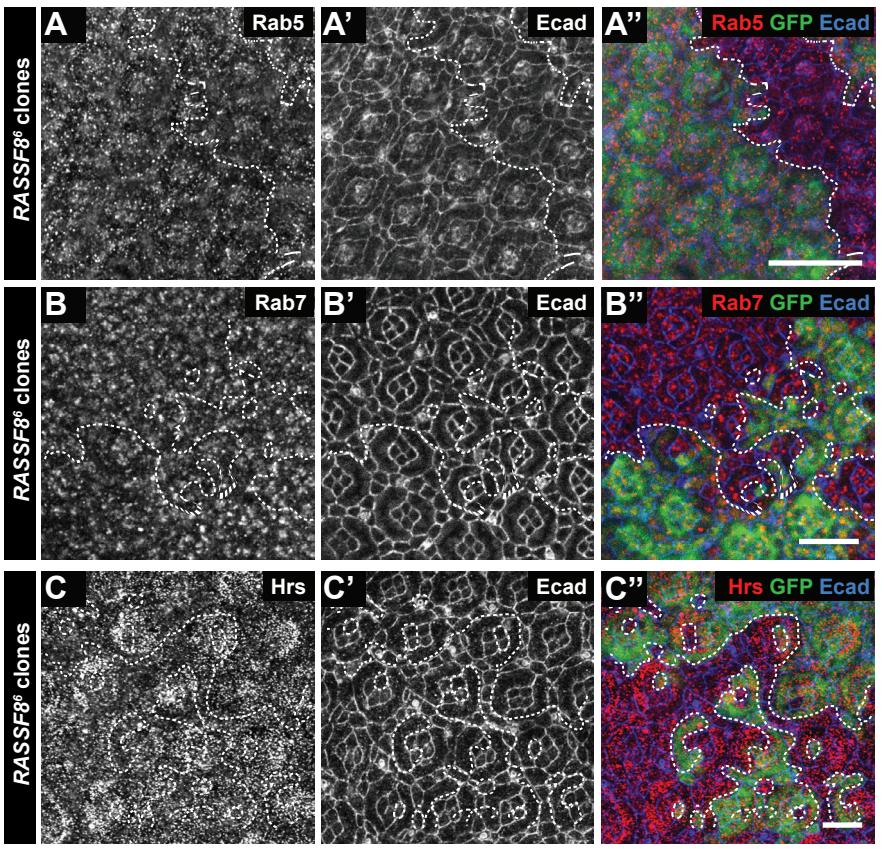

Fig. S3. Normal Rab5, Rab7 and Hrs localisation in *RASSF8* retinal clones

(A-C'') Confocal micrographs of pupal retinas at 26 hours APF bearing *RASSF8* mutant clones generated using *eyFLP* and stained as indicated. White dotted lines label the clone boundaries. Staining for Rab5 (A-A''), Rab7 (B-B'') and Hrs (C-C'') is not altered in *RASSF8* mutant pupal retina clones marked by the absence of GFP. Scale bars: 10 µm.

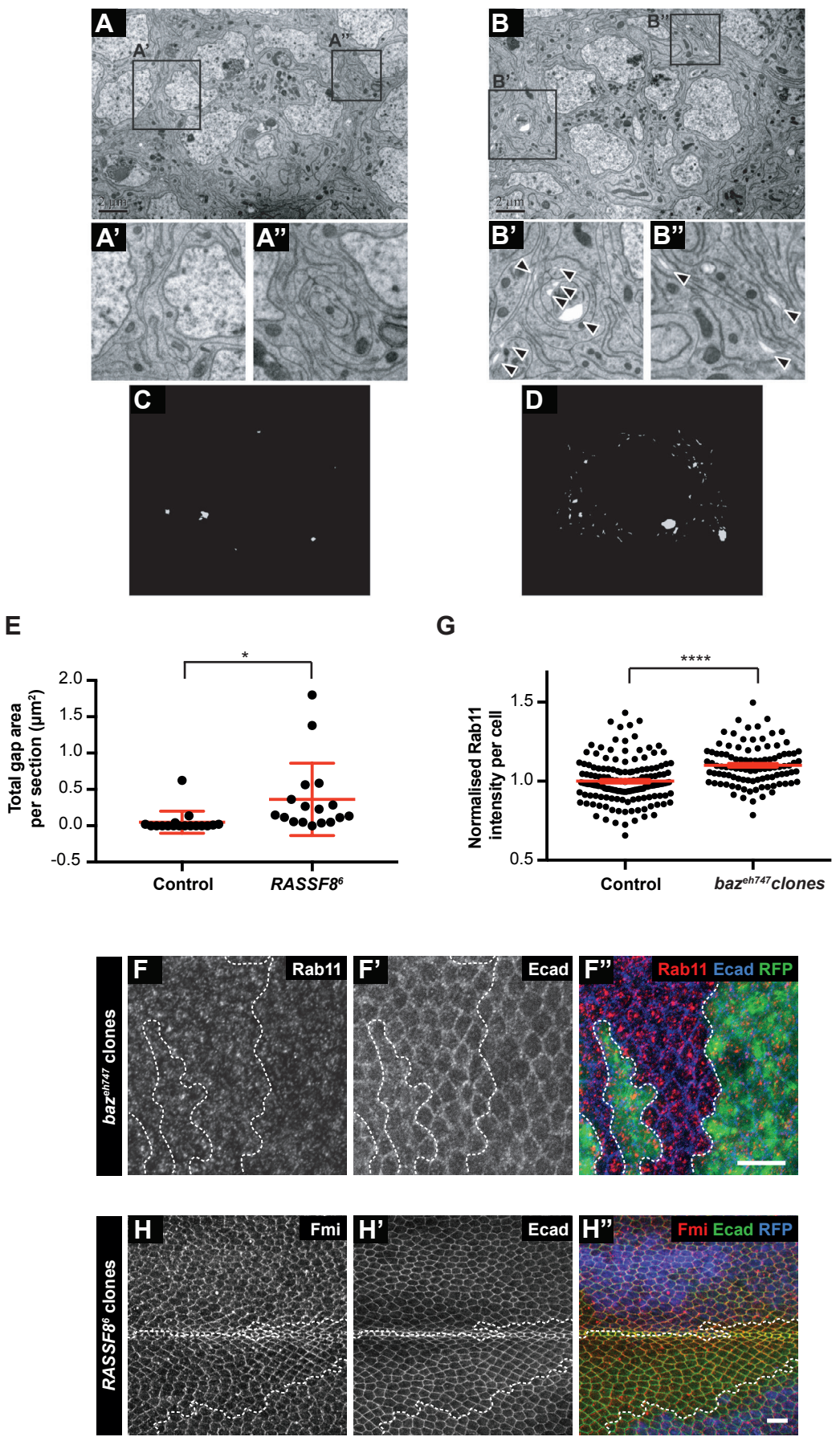

Fig. S4. Intercellular gaps in *RASSF8* mutant pupal retinas

Electron micrographs reveal a defect in cell-cell adhesion in *RASSF8* mutant retinas at 26 hours APF. TEM of control (A) and *RASSF8* mutant (B) ommatidia at the level of the apical AJs reveals an increase in gaps at cell-cell junctions. Inserts of representative areas show an absence of gaps in control (A'-A'') and numerous gaps in the mutant (arrows) (B' and B''). The gaps in ommatidia from single plane images (n = 17 images) were quantified by manual segmentation in Amira. The resulting segmentations are shown as a projection of the non-sequential overlaid images for control (C) and mutant (D). (E) Quantification of gap area per section in control and *RASSF8* mutant retinas. Error bars = s.d.; n=17. Two-tailed Student's t-test, * p = 0.0186. Scale bars in A and B: 2 µm. (F-F") Staining for Rab11 (red) is only modestly increased in *baz* mutant pupal wing clones marked by the absence of RFP (green). Ecad staining is in blue. (G) Quantification of the total intracellular Rab11 fluorescence per cell in control (RFP+) or *baz* mutant (RFP-) cells. The *baz* mutant values were normalised to the control values. Error bars = s.e.m.; n=101-149 cells from 3 different wings. Two-tailed Student's t-test: **** p<0.0001. Scale bar: 10 µm. See Table S2 for raw data. (H-H'') *RASSF8* mutant pupal wing clones at 30 hours APF marked by absence of GFP (green stained with anti-Fmi antibody. Polarised staining of Fmi is normal in RASSF8 and is concentrated on the proximal and distal cell boundaries.

Table S1. Raw data and statistics for Figures 1 and S1

Click here to download Table S1

Table S2. Raw data and statistics for Figures 5 and S4

Click here to download Table S2